© 2021. Published by The Company of Biologists Ltd | Development (2021) 148, dev199585. doi:10.1242/dev.199585

RESEARCH ARTICLE

Δ9-Tetrahydrocannabinol inhibits Hedgehog-dependent patterning during development

Hsiao-Fan Lo[1], Mingi Hong[1], Henrietta Szutorisz[2], Yasmin L. Hurd[2] and Robert S. Krauss[1,*]

ABSTRACT

Many developmental disorders are thought to arise from an interaction between genetic and environmental risk factors. The Hedgehog (HH) signaling pathway regulates myriad developmental processes, and pathway inhibition is associated with birth defects, including holoprosencephaly (HPE). Cannabinoids are HH pathway inhibitors, but little is known of their effects on HH-dependent processes in mammalian embryos, and their mechanism of action is unclear. We report that the psychoactive cannabinoid Δ9-tetrahydrocannabinol (THC) induces two hallmark HH loss-of-function phenotypes (HPE and ventral neural tube patterning defects) in *Cdon* mutant mice, which have a subthreshold deficit in HH signaling. THC therefore acts as a 'conditional teratogen', dependent on a complementary but insufficient genetic insult. *In vitro* findings indicate that THC is a direct inhibitor of the essential HH signal transducer smoothened. The canonical THC receptor, cannabinoid receptor-type 1, is not required for THC to inhibit HH signaling. Cannabis consumption during pregnancy may contribute to a combination of risk factors underlying specific developmental disorders. These findings therefore have significant public health relevance.

KEY WORDS: THC, Cannabis, Hedgehog, Holoprosencephaly, Birth defect, CDON, Mouse

INTRODUCTION

Congenital malformations affect approximately 8 million newborns worldwide each year and are a leading cause of death for infants and children of all ages (Christianson et al., 2006; Krauss and Hong, 2016; Wallingford, 2019). In some cases, mutations in single genes or exposure to individual teratogens is sufficient to cause a developmental disorder in most or all those affected (Amberger et al., 2019; Gilbert-Barness, 2010; Webber et al., 2015). For many of the most common structural birth defects, however, a single causative factor cannot be identified, and the underlying etiology for such disorders is poorly understood. In these cases, it is likely that genetic and environmental risk factors interact to elevate the chance of a defect occurring in specific developmental processes (Beames and Lipinski, 2020; Fraser, 1980; Krauss and Hong, 2016; Lovely et al., 2017). Genome sequencing has led to identification of numerous birth defect-associated variants, many of which appear to predispose individuals to a given anomaly and presumably act with additional factors (Webber et al., 2015). Identification of subthreshold environmental risk factors by epidemiology is more difficult.

Cannabis is the illicit drug most commonly used during pregnancy and, with expanded legalization and decreased perception of risk, use is increasing (Volkow et al., 2017; Young-Wolff et al., 2017). Meta-analysis of studies through 2014 concluded that maternal cannabis use is associated with low birth weight and increased likelihood of requirement for neonatal intensive care (Gunn et al., 2016). Recently, in Colorado, a correlation was reported between: (1) increased cannabis usage during pregnancy; (2) increased fetal phytocannabinoid exposure levels; and (3) an increase in major structural developmental defects (Reece and Hulse, 2019). Use of other drugs and tobacco remained static or fell in Colorado during the reporting period. A similar pattern was observed with rising incidence of atrial septal defects in multiple US states and Australia (Reece and Hulse, 2020). These correlations suggest that cannabinoids might be teratogenic, but they do not demonstrate causality.

A common birth defect that serves as a model for gene-environment interactions and multifactorial etiology is holoprosencephaly (HPE) (Beames and Lipinski, 2020; Hong and Krauss, 2018; Roessler et al., 2018). HPE is caused by failure to define the midline of the forebrain and/or midface. HPE comprises a phenotypic continuum ranging from complete failure to partition the forebrain into hemispheres with accompanying cyclopia, through to mild midfacial midline deficiency (Cohen, 2006; Muenke and Beachy, 2001). The Hedgehog (HH) signaling pathway is a key regulator of many developmental processes, including patterning of the forebrain and facial midline, limbs and digits, and ventral neural tube (VNT) (Petryk et al., 2015; Sagner and Briscoe, 2019; Tickle and Towers, 2017). HPE is associated with heterozygous mutations in the HH pathway (Dubourg et al., 2018; Roessler et al., 2018). Clinical presentation of HPE is highly variable, and many mutation carriers are unaffected, even in pedigrees. These observations have led to a multifactorial, 'mutation plus modifier' model, in which heterozygous mutations may be insufficient for severe phenotypes and their penetrance and expressivity are graded by additional genetic variants and/or environmental exposures (Dubourg et al., 2018; Hong and Krauss, 2018; Roessler et al., 2012).

HH ligands activate a conserved signaling pathway (Kong et al., 2019; Lee et al., 2016; Petrov et al., 2017). In the absence of HH, the primary receptor patched 1 (PTCH1) acts to inhibit the activity of a second membrane protein, smoothened (SMO). Binding of HH to PTCH1 relieves inhibition of SMO. SMO then signals to activate pathway target genes via GLI transcription factors. SMO is a class F, G protein-coupled receptor (GPCR). PTCH1 appears to function as a transporter to restrict accessibility of SMO to its activating ligands, namely cholesterol and oxysterols. HH ligands block PTCH1

[1]Department of Cell, Developmental, and Regenerative Biology, New York, NY 10029, USA. [2]Addiction Institute and Departments of Psychiatry and Neuroscience, Icahn School of Medicine at Mount Sinai, New York, NY 10029, USA.

*Author for correspondence (Robert.Krauss@mssm.edu)

R.S.K., 0000-0002-7661-3335

Handling Editor: James Briscoe
Received 3 March 2021; Accepted 23 August 2021

Development (2021) 148, dev199585. doi:10.1242/dev.199585

function, allowing SMO access to cholesterol and oxysterols, thus activating SMO signaling (Qi and Li, 2020; Radhakrishnan et al., 2020). These events occur in the primary cilium, an organelle in which HH pathway components are trafficked and concentrated for signaling (Bangs and Anderson, 2017; Gigante and Caspary, 2020). Consistent with the notion that SMO is itself a ligand-regulated receptor, many small molecules that act as SMO agonists or antagonists have been identified (Sharpe et al., 2015). Although PTCH1 function is sufficient for SMO inhibition, HH signal reception also requires at least one of three co-receptors (CDON, BOC, GAS1). CDON, BOC and GAS1 have overlapping roles and are collectively required for HH signaling (Allen et al., 2011; Izzi et al., 2011; Wierbowski et al., 2020; Zhang et al., 2011). Mice with targeted mutations in any one of these co-receptors have a selective and partial loss of HH pathway function.

In a search for endogenous lipids that act as SMO antagonists, Eaton and colleagues identified endocannabinoids as inhibitors of HH signaling (Khaliullina et al., 2015). Endocannabinoids were effective as HH pathway inhibitors in both developing *Drosophila* wing disks and cultured mammalian cells. Endocannabinoids are fatty acids/alcohols linked to polar head groups that signal through the GPCRs cannabinoid receptor-type 1 (CB1R; CNR1) and -type 2 (CB2R; CNR2) (Lu and Mackie, 2020; Maccarrone et al., 2015). Phytocannabinoids are bioactive ingredients of cannabis and include Δ9-tetrahydrocannabinol (THC) and cannabidiol (CBD), the former being the major psychoactive component. These compounds exert their effects via CB1R, CB2R, and/or other receptors, with CB1R responsible for mediating the major neurobehavioral effects of THC (Lu and Mackie, 2020; Schurman et al., 2020). Importantly, THC and CBD inhibit HH signaling in a similar manner to endocannabinoids, whereas structurally unrelated CB1R and CB2R agonists/antagonists do not (Khaliullina et al., 2015). Cannabinoids have been proposed to inhibit HH signaling at the level of SMO, although this mechanism was not uniform among those analyzed and has been questioned by others (Sever et al., 2016).

These findings raise the possibility that *in utero* exposure to phytocannabinoids might be teratogenic, owing to an ability to inhibit HH signaling at crucial points during development. We report here that THC is teratogenic to genetically sensitized mice harboring a subthreshold deficit in HH pathway signaling strength. THC dose-dependently induced HH loss-of-function phenotypes, including HPE, in these mice but not in wild-type mice. THC therefore acted as a 'conditional teratogen', dependent on a complementary but insufficient genetic insult. Furthermore, in *in vitro* assays, THC displayed properties similar to the *bone fide* SMO inhibitor SANT1. Together, these results raise the possibility that human cannabis consumption during early pregnancy may expose embryos to HH inhibition, presenting an environmental risk factor for birth defects.

RESULTS

THC-exposed *Cdon*$^{-/-}$ embryos display HPE with craniofacial midline defects

Cdon$^{-/-}$ mice on a 129S6 background have a subthreshold defect in HH signaling and are sensitive to induction of HPE by both genetic and environmental modifiers (Hong and Krauss, 2018). They therefore model human HPE and are an ideal model in which to assess THC teratogenicity. 129S6 *Cdon*$^{+/-}$ mice were intercrossed and pregnant females received a single dose of THC at 5, 10 or 15 mg/kg, administered intraperitoneally at embryonic day (E) 7.5. The E7.5 time point was used because it was most effective for induction of HPE in wild-type mice by the potent SMO inhibitor vismodegib (Heyne et al., 2015). We measured blood concentrations of THC and metabolites in pregnant female mice, and the peak levels achieved at the highest THC dose used were similar to those achieved by humans after inhalation of 34 mg cannabis (180-200 ng/ml) (Grotenhermen, 2003) (Fig. S1).

Embryos were harvested at E14 and scored as positive for HPE if they displayed a fused upper lip, an unambiguous phenotype without gradation that arises as a consequence of defective craniofacial midline patterning (Hong and Krauss, 2012). Vehicle- and THC-treated *Cdon*$^{+/+}$ and *Cdon*$^{+/-}$ embryos did not have HPE, nor did vehicle-treated *Cdon*$^{-/-}$ embryos. In contrast, THC-exposed *Cdon*$^{-/-}$ embryos displayed mid-facial HPE phenotypes in a dose-responsive manner (Fig. 1A,B; Table S1). Hematoxylin and Eosin (H&E)-stained sections revealed that THC-treated *Cdon*$^{-/-}$ embryos had fully partitioned forebrains, but displayed substantial diminution of midfacial structures, including close-set and rudimentary vomeronasal organs, and reduced width of the nasal septum cartilage (Fig. 1A-A‴; Fig. S2). These results classify THC-induced HPE in *Cdon*$^{-/-}$ mice as the relatively mild, lobar category (Krauss, 2007). Whole-mount *in situ* hybridization at E10 revealed reduction in expression of two direct SHH target genes, *Gli1* and *Nkx2-1,* in the rostroventral midline of THC-treated *Cdon*$^{-/-}$ embryos (Fig. 1C).

To investigate the effects of THC on gene expression more quantitatively, RNA was extracted from dissected forebrains of E9.0 embryos, and quantitative RT-PCR (qRT-PCR) was performed for several SHH target genes. Although there was some variability, possibly related to partial penetrance, mRNA levels of *Gli1*, *Nkx2-1* and *Shh* were significantly reduced in THC-treated *Cdon*$^{-/-}$ embryos (Fig. 1D). *Ptch1* mRNA levels trended lower in THC-treated *Cdon*$^{-/-}$ embryos, although this was not statistically significant owing to variability between the samples (P=0.08). In contrast, levels of *Bmp4* mRNA, which controls CNS patterning dorsally and medially and is not known to be directly regulated by HH signaling, was similar between controls and THC-treated *Cdon* mutants (Fig. 1D). Additionally, these results may underestimate the reduction in expression of SHH target genes in the most affected region of THC-treated *Cdon*$^{-/-}$ embryos because non-midline structures were by necessity present in the dissected tissue. Taken together, these results show that *Cdon* mutation and THC synergized to induce HPE in mice.

THC induces VNT patterning defects in *Cdon*$^{-/-}$ mice

We next sought to assess the effects of *in utero* exposure to THC on a second HH-dependent patterning process. Sonic HH (SHH) produced by the notochord and floor plate (FP) forms a ventral-to-dorsal gradient of pathway activity in the developing neural tube. In response to distinct levels of SHH pathway activity, expression of specific transcription factors is induced in specific progenitor zones of the VNT. These proteins include: FOXA2 (in the FP), NKX2-2 (in p3 progenitors) and OLIG2 (in pMN motor neuron progenitors). Pregnant dams were treated with a single dose of THC (15 mg/kg) at E8.0 and embryos were analyzed at E9.5, by immunofluorescence (IF) analysis of forelimb-level sections. The E8.0 time point was used because it was effective for inhibition of SHH-dependent VNT patterning in wild-type embryos by the SMO inhibitor cyclopamine (Ribes et al., 2010). THC reduced the number of FOXA2^{+} FP cells by >50% and of NKX2-2^{+} p3 progenitors by >35% in *Cdon*$^{-/-}$ embryos (Fig. 2). The more dorsally positioned OLIG2^{+} pMN progenitors, which require a lower level of HH signal to be induced, were not affected (Fig. 2). These results are very similar to those

Development (2021) 148, dev199585. doi:10.1242/dev.199585

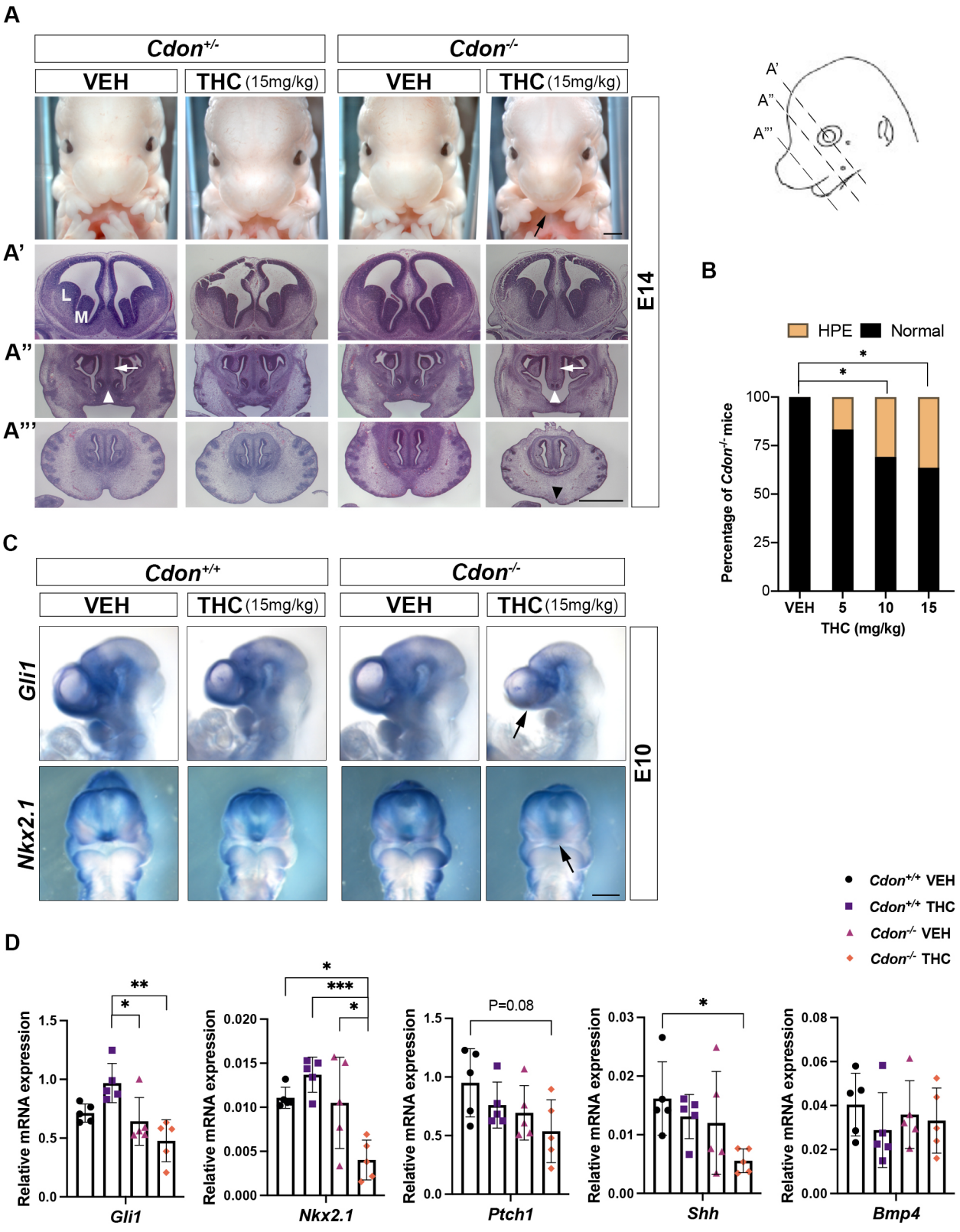

Fig. 1. See next page for legend.

obtained by removal of one copy of *Shh* from *Cdon*$^{-/-}$ mice (Tenzen et al., 2006). Taken together, our findings demonstrate that THC is teratogenic in genetically sensitized mice, producing two well-established, SHH loss-of-function phenotypes: HPE and defective VNT patterning.

THC is likely a direct inhibitor of SMO

Khaliullina et al. reported that THC inhibited a HH-dependent reporter construct in NIH3T3 cells, a well-established cell culture system for studying HH signaling and the mechanisms of pathway inhibitors (Khaliullina et al., 2015; Taipale et al., 2000). We

Development (2021) 148, dev199585. doi:10.1242/dev.199585

Fig. 1. THC induces HPE in *Cdon*$^{-/-}$ mutant mice. (A-A‴) Frontal views of forebrains and faces of embryos with indicated genotypes and treatments. HPE phenotypes in THC-treated *Cdon*$^{-/-}$ mice include fusion of the upper lip (black arrow), close-set and rudimentary vomeronasal organs (white arrowheads), reduced nasal septal cartilage (white arrows) and loss of midfacial midline structure (black arrowhead). Mice were administered THC or vehicle (VEH) at E7.5 and harvested at E14. Top row: whole-mount E14 embryos. Next three rows: H&E-stained sections of E14 embryos. L, lateral ganglionic eminence; M, medial ganglionic eminence. The angle and level of H&E sections are displayed in the diagram on the right, as A′, A″ and A‴. (B) THC induces HPE in *Cdon*$^{-/-}$ mice in a dose-dependent manner. The numbers of embryos scored as positive for HPE were 2/12, 4/13 and 4/11 at 5 mg/kg, 10 mg/kg and 15 mg/kg THC, respectively; also see Table 1. **P*<0.05 (two-tailed Fischer's exact test). (C) Whole-mount *in situ* hybridization of E10 embryos exposed *in utero* to THC (15 mg/kg) or VEH. Expression of two direct SHH target genes (*Gli1* and *Nkx2-1*) is reduced in the rostroventral midline (arrows). Embryos had 30-35 pairs of somites. (D) Inhibition of SHH target gene expression by THC. Pregnant females were administered 15 mg/kg THC or VEH at E8.0 and embryos of the indicated genotypes assessed. Embryo forebrains were isolated at E9.0 (17-20 pairs of somites) for qRT-PCR analysis of *Gli1*, *Nkx2-1*, *Ptch1*, *Shh* and *Bmp4* expression, all normalized to *Gapdh* expression. Values are mean±s.d. from five individual embryos **P*<0.05, ***P*<0.01, ****P*<0.001 (ordinary one-way ANOVA). Scale bars: 1 mm.

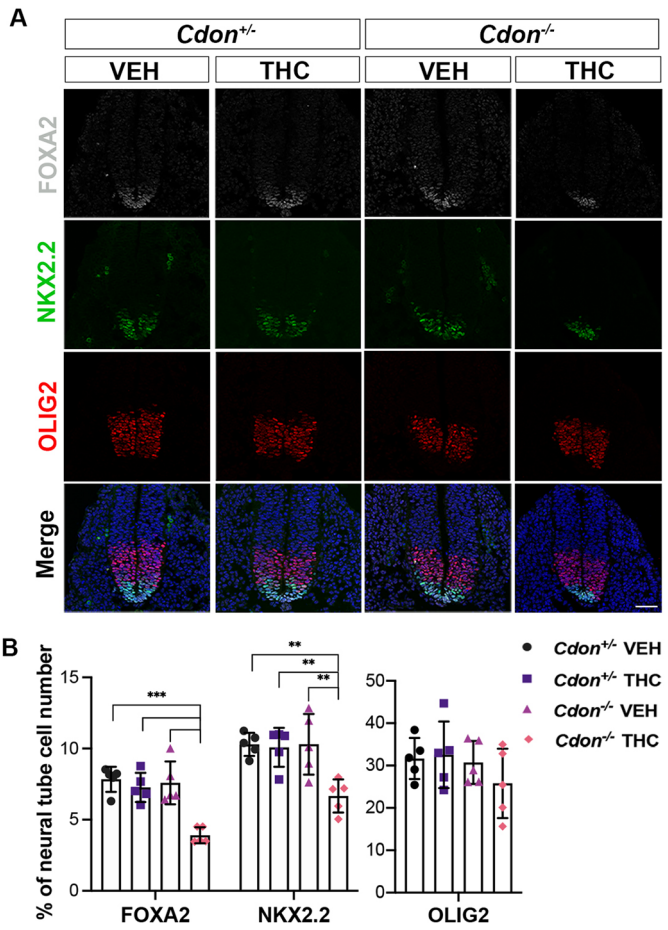

Fig. 2. THC induces VNT patterning defects. (A) Immunofluorescence analysis of forelimb level sections of embryos with indicated genotypes. Pregnant females were administered 15 mg/kg THC or VEH at E8.0 and analyzed at E9.5 (20-24 pairs of somites). All nuclei are visible by DAPI stain (blue) in the merged images. Scale bar: 50 µm. (B) Numbers of FOXA2^{+}, NKX2-2^{+} and OLIG2^{+} cells relative to whole neural tube cells were quantified. Values are means from three to five sections from five individual mice. ***P*<0.05, ***P*<0.01, ****P*<0.001 (ordinary one-way ANOVA with Tukey's multiple comparison test). See Table S2 for numbers of FOXA2^{+}, NKX2-2^{+}, OLIG2^{+} and total cells in neural tubes of individual embryos.

confirmed this observation. Treatment of NIH3T3 cells with recombinant SHH induced an ∼10-fold increase in expression of the direct, endogenous target gene *Gli1* as measured by qRT-PCR (Fig. 3A). THC dose-dependently inhibited *Gli1* induction in response to SHH, with an IC_{50} of ∼1 µM. Similar results were obtained when these cells were stimulated with the direct SMO agonist SAG (Fig. S3A), and with SHH treatment of a second cell system, freshly prepared mouse embryo fibroblasts (MEFs) (Fig. S3B).

It has been reported that cannabinoids inhibit HH signaling at the level of SMO, although differences were seen between the cannabinoids examined, and THC was not tested (Khaliullina et al., 2015). PTCH1 and SUFU are negative regulators of HH signaling. MEFs that are null for either gene display constitutive pathway activity, with PTCH1 functioning upstream of SMO, and SUFU acting downstream of SMO (Kong et al., 2019; Lee et al., 2016; Petrov et al., 2017). To identify the position within the HH pathway at which THC acts, we first tested its ability to inhibit constitutive expression of *Gli1* in *Ptch1*$^{-/-}$ and *Sufu*$^{-/-}$ MEFs. THC attenuated *Gli1* expression in *Ptch1*$^{-/-}$ MEFs, but not in *Sufu*$^{-/-}$ MEFs, in a dose-dependent manner (Fig. 3B). Therefore, THC modulates SHH signaling downstream of PTCH1 and upstream of SUFU. Although these data place the likely point of action of THC at the level of SMO, this could occur via direct SMO inhibition or indirectly, e.g. via perturbation of primary cilia, the cellular site of signaling to GLI.

SMO activation is a two-step process. Ciliary transport of SMO (step 1) is followed by SMO activation within cilia (step 2) (Fig. 3C) (Rohatgi et al., 2009; Wilson et al., 2009). A low level of SMO trafficks through primary cilia constitutively. Some direct SMO inhibitors, such as SANT1, induce a SMO conformation that inhibits trafficking and prevents ciliary accumulation in response to activators, such as SHH and SAG. Another class of SMO inhibitor, exemplified by cyclopamine, induces a SMO conformation that does not inhibit trafficking, but which resists activation within cilia. Therefore, cyclopamine-type inhibitors trap SMO in primary cilia even in the absence of SHH or SAG, yet block activation of SMO within cilia, even in the presence of these pathway activators (Rohatgi et al., 2009; Wilson et al., 2009). We assessed the effect of THC on ciliary translocation of endogenous SMO in NIH3T3 cells treated with various HH pathway-regulating compounds (Fig. 3D,E; Table 1). The percentage of cells with ciliary SMO and fluorescence intensity of ciliary protein expression were determined. THC alone did not trigger SMO translocation to cilia, but it blocked SMO accumulation in cilia in response to SHH, cyclopamine or SAG. THC also inhibited constitutive ciliary localization of SMO in *Ptch1*$^{-/-}$ MEFs. THC did not affect cilium length or ciliary levels of the primary cilia marker ARL13B (Fig. S4A,B). Therefore, THC acts similarly to SANT1, preventing SMO translocation into primary cilia.

The phytocannabinoid CBD is structurally related to THC and has also been reported to inhibit HH signaling (Khaliullina et al., 2015). In contrast to our results with THC, Khaliullina et al. found that CBD did not prevent localization of exogenously expressed SMO to primary cilia in response to SAG (Khaliullina et al., 2015). Because these results and our own findings with THC were dichotomous, we tested CBD as well. CBD inhibited SHH-induced *Gli1* expression in NIH3T3 cells with an IC_{50} of ∼1.2 µM, a value similar to that of THC (Fig. 4A). Like THC, CBD alone did not promote translocation of SMO to primary cilia (Fig. 4B,C). We found that CBD did reduce endogenous SMO ciliary translocation in response to SHH. However, despite having similar IC50 values,

Development (2021) 148, dev199585. doi:10.1242/dev.199585

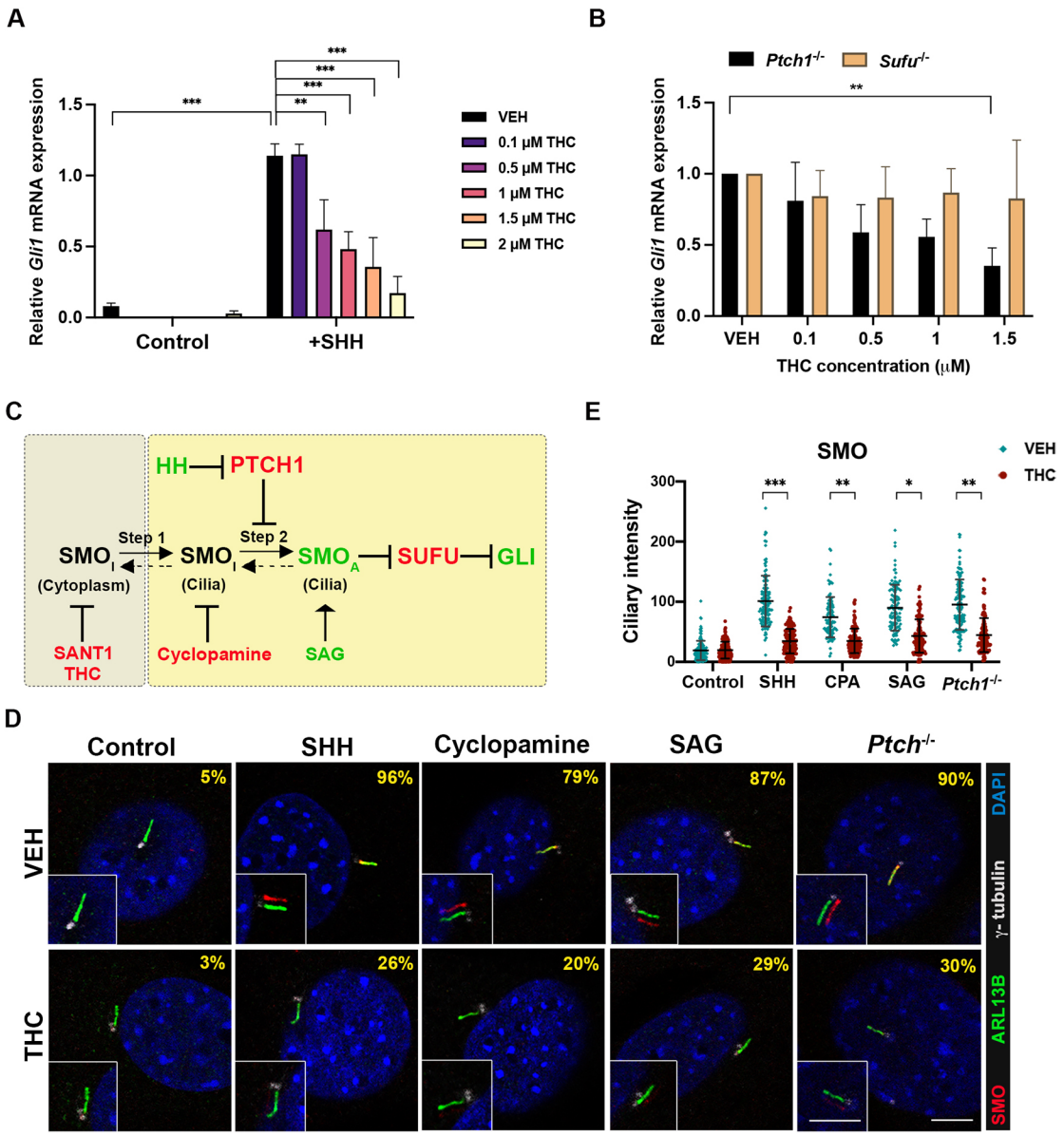

Fig. 3. THC inhibits HH signaling at the level of SMO. (A) NIH3T3 cells were treated with 5 ng/ml SHH and the indicated concentrations of THC for 24 h. Relative endogenous *Gli1* mRNA expression was analyzed by qRT-PCR and normalized to *Gapdh* levels. Values are mean±s.d., n=3. *P<0.05, **P<0.01, ***P<0.001 (ordinary one-way ANOVA with Tukey's multiple comparison test). (B) THC inhibits endogenous *Gli1* expression in *Ptch1*$^{-/-}$, but not *Sufu*$^{-/-}$, MEFs. Relative *Gli1* mRNA expression was determined by qRT-PCR and normalized to *Gapdh* levels. Values are mean±s.d., n=3. **P<0.01 (ordinary one-way ANOVA with Tukey's multiple comparison test). (C) SMO activation is a two-step process: ciliary transport of inactive SMO (SMO_I) (step 1) is followed by SMO activation (SMO_A) within cilia (step 2). Pathway agonists (green) and antagonists (red) can control SMO transport entry or exit steps. (D) THC blocks endogenous SMO localization in primary cilia in NIH3T3 cells in response to multiple stimuli. Primary cilia are marked by ARL13B; γ-tubulin marks centrioles. The percentage of cells with cilium-localized SMO is displayed in the top right. See Table 1 for detailed quantification. In insets, the SMO and ARL13B signal overlay is shifted for easy visualization. SHH was used at 5 ng/ml, cyclopamine at 5 µm, SAG at 100 nM, and THC at 1.5 µM. (E) Quantification of SMO fluorescence intensity in primary cilia. Values are mean±s.d. Each point represents an individual cell collated from at least three independent experiments. *P<0.05, **P<0.01, ***P<0.001 (Student's t-test). Scale bars: 5 µm.

CBD was significantly less effective than THC in reducing: (1) the percentage of cells with SMO^+ cilia; and (2) the steady-state amount of SMO within SMO^+ cilia, in SHH-treated cells (Fig. 4B,C; Table 1). CBD did not affect cilium length or ciliary levels of the primary cilia marker ARL13B (Fig. 4C). CBD may therefore inhibit HH signaling by a mechanism somewhat distinct from either SANT1-type or cyclopamine-type SMO inhibitors.

To identify whether THC may be a direct inhibitor of SMO, we measured its ability to compete with a fluorescent derivative of cyclopamine (Bodipy-CPA) for binding to SMO (Chen et al., 2002). We transfected HEK293 cells with an expression vector encoding Myc epitope-tagged SMO or with an empty vector as a control. SMO-Myc-expressing cells, but not control cells, displayed strong Bodipy-CPA binding (Fig. 5). SANT1 and KAAD-cyclopamine (a potent analog of cyclopamine) each competed with Bodipy-CPA for SMO binding (Fig. 5). THC at 10 µM, but not 1 µM, also inhibited Bodipy-CPA binding (Fig. 5). In contrast, 10 µM CBD did not significantly diminish Bodipy-CPA binding to SMO-expressing cells (Fig. 5). Although 10 µM is a high concentration of THC, cholesterol (an endogenous SMO ligand)

Development (2021) 148, dev199585. doi:10.1242/dev.199585

Table 1. Effects of THC and CBD on SMO localization to primary cilia

	Ciliary SMO$^+$/ total cell number	Percentage of cells with ciliary SMO$^+$	*P*-value with *t*-test (versus VEH)	*P*-value with *t*-test (versus THC)
Control+VEH	7/131	4.5±3.3%		
Control+THC	3/128	3.1±4.9%	ns	
SHH+VEH	110/116	96.1±5%		
SHH+THC	33/127	25.8±4.7%	*P*<0.001	
CPA+VEH	78/100	79.2±4.5%		
CPA+THC	20/101	21.2±2.5%	*P*<0.001	
SAG+VEH	91/105	86.8±5.8%		
SAG+THC	32/105	28.9±21.6%	*P*<0.05	
Ptch1$^{-/-}$+VEH	120/130	90±2.6%		
Ptch1$^{-/-}$+THC	41/130	29.9±6.3%	*P*<0.001	
Control+VEH	6/117	5.3±1.5%		ns
Control+CBD	5/116	3.7±3%	ns	ns
SHH+VEH	97/109	89.3±3%		ns
SHH+CBD	80/117	67.6±5.6%	*P*<0.01	*P*<0.001

ns, not significant; VEH, vehicle.
All experiments were performed with NIH3T3 cells, except those noted as using *Ptch1*$^{-/-}$ MEFs. SHH was used at 5 ng/ml, cyclopamine at 5 µM, SAG at 100 nM, THC and CBD at 1.5 µM.

competed with Bodipy-CPA in a similar concentration range (Huang et al., 2016). Furthermore, the fact that CBD, a close structural congener of THC, was not effective at this dose argues that the ability of THC to compete with Bodipy-CPA is specific.

CB1R is not required for THC-mediated inhibition of HH signaling

The psychoactive effects of THC are exerted via CB1R, encoded by the gene *Cnr1* (Lu and Mackie, 2020). It has been proposed that cannabinoids inhibit HH signaling via CB1R-SMO heterodimers (Fish et al., 2019). We sought to explore this possibility further. First, if CB1R is required for cannabinoids to inhibit SMO, CB1R must be expressed in cells that display a cannabinoid-sensitive HH response. NIH3T3 cells and MEFs are HH responsive, and THC inhibits this response (Fig. 3A; Figs. S3A,B). However, we did not detect *Cnr1* mRNA or CB1R protein in either cell type, whereas they were easily detected in mouse whole-brain lysate (Fig. 6A,B).

We next performed IF analysis for CB1R on VNT sections from embryos collected at E8.5 (both neural fold and early NT stages), E9.5, E10.5 and E11.5. CB1R was detected in some cells of the ventricular zone at the neural fold stage, consistent with previous reports (Gilbert et al., 2015; Psychoyos et al., 2012). However, little to no specific CB1R IF signal was observed in the developing VNT at E8.5 early neural tube stage, E9.5 or E10.5, with the exception of a few cells at the ventricular edge of the floor plate that reproducibly exhibited a strong signal (Fig. 6C). Robust CB1R expression was observed at E11.5, but this was localized to the HH-non-responsive mantle domain, which contains more differentiated neurons (Fig. 6C). These results demonstrate that CB1R levels are very low in VNT cells at developmental stages when they are undergoing THC-sensitive, SHH-dependent neuronal patterning. These findings are consistent with mRNA *in situ* hybridization data

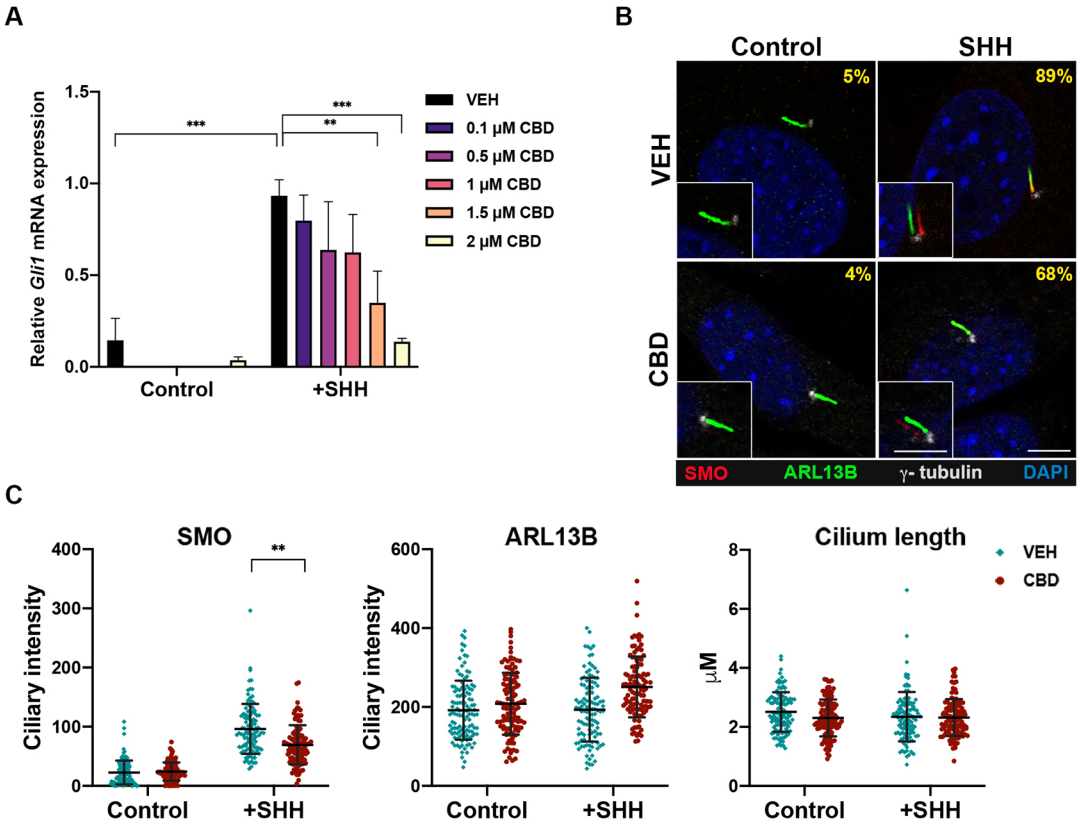

Fig. 4. CBD inhibits SHH pathway activation and reduces SMO localization in primary cilia. (A) CBD dose-dependently inhibited SHH-stimulated *Gli1* expression in NIH3T3 cells. Values are mean±s.d., *n*=3. ***P*<0.01, ****P*<0.001 (ordinary one-way ANOVA with Tukey's multiple comparison test). (B) The percentage (top right of each panel) of SMO$^+$ cilia in SHH-stimulated cells was modestly decreased by CBD. See Table 1 for complete quantification. Insets show the SMO and ARL13B signal overlay shifted for easy visualization. SHH was used at 5 ng/ml and CBD at 1.5 µM. Scale bars: 5 µm. (C) Quantification of SMO and ARL13B fluorescence intensity in primary cilia. Cilia length was also measured. Values are mean±s.d. Each point represents an individual cell collated from three different experiments. ***P*<0.01 (Student's *t*-test).

Development (2021) 148, dev199585. doi:10.1242/dev.199585

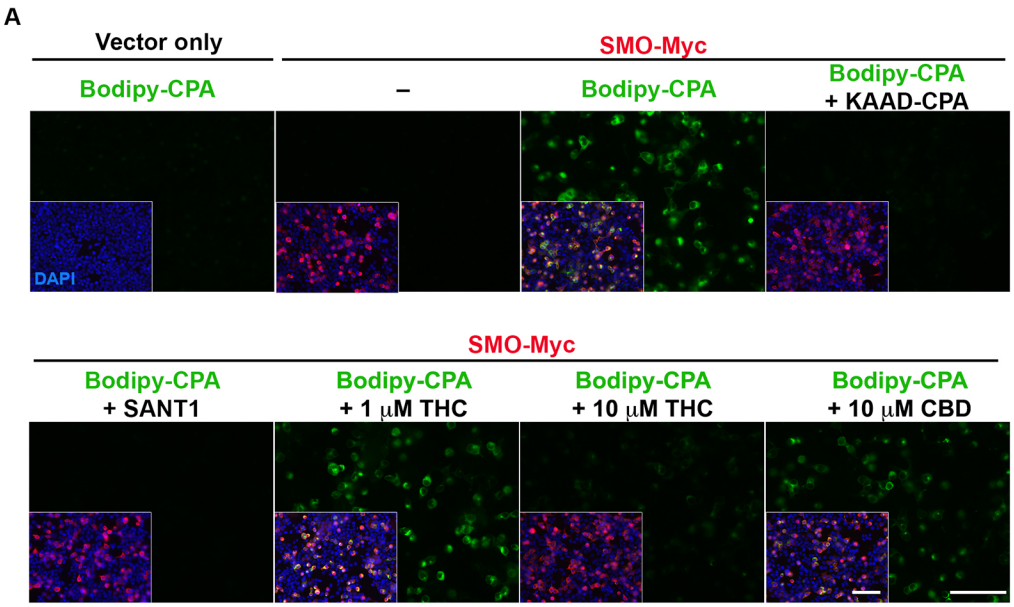

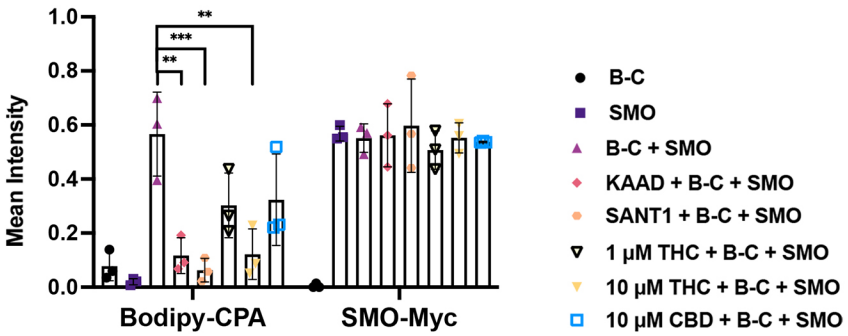

Fig. 5. THC, but not CBD, competes with Bodipy-cyclopamine for binding to SMO. (A) HEK293T cells were transfected with SMO-Myc (red in insets) or empty vector. Cells were then incubated with Bodipy-cyclopamine (Bodipy-CPA; green), in the presence or absence of different competitors as indicated. Bodipy-CPA was used at 5 nM, KAAD-CPA at 200 nM, SANT1 at 1 µM, and THC and CBD as indicated. Scale bars: 100 µm. (B) Quantification of Bodipy-CPA and SMO-Myc fluorescence intensity. $^{**}P<0.01$, $^{***}P<0.001$(ordinary one-way ANOVA with Tukey's multiple comparison test). Values represent mean±s.d., from three independent experiments.

showing a lack of *Cnr1* expression at similar stages in the chick VNT (Watson et al., 2008), patterning of which closely resembles the mouse VNT (Dessaud et al., 2008). In general, *Cnr1* expression follows neuronal differentiation (Watson et al., 2008), consistent with our IF results in the VNT. Our IF with CB1R antibodies was further validated by staining sections of E14 cerebral cortex (Fig. 6C), which reproduced localization patterns similar to those previously reported (Mulder et al., 2008).

We next attempted to co-immunoprecipitate CB1R and SMO. Extracts of E14 and adult mouse brains were immunoprecipitated with antibodies to CB1R and then blotted for CB1R and SMO. CB1R and SMO were detected in whole lysates by western blot. However, although CB1R was efficiently immunoprecipitated, SMO was not detectable in these precipitates (Fig. 6D).

Finally, to test for effects of CB1R in THC-mediated inhibition of HH signaling, we established NIH3T3 cells that expressed CB1R in a doxycycline-inducible manner. We reasoned that if CB1R levels were rate-limiting for the inhibition of HH signaling by THC, exogenous expression of CB1R in NIH3T3 cells would sensitize them to THC-mediated attenuation of SHH-induced expression of *Gli1*. Treatment of these cells with 0.05 µg/ml doxycycline induced CB1R expression to a level similar to that seen in Neuro-2a cells, which display CB1R-dependent signaling in response to cannabinoids (Graham et al., 2006; He et al., 2005) (Fig. S5A). CB1R expression did not alter the ability of THC to dose-dependently inhibit *Gli1* mRNA induction in response to SHH stimulation (Fig. 6E). Furthermore, CB1R was not present in primary cilia, in control, THC-, SHH- or THC+SHH-treated cells (Fig. S5B). Taken together, we conclude that CB1R is not required for THC-mediated inhibition of HH signaling.

DISCUSSION

We report here that THC is teratogenic in genetically sensitized mice (129S6 *Cdon*$^{-/-}$ mice). A single *in utero* dose of THC resulted in two hallmark HH loss-of-function phenotypes: HPE and VNT patterning defects. *In vitro* experiments argue that THC exerted these effects as a direct, albeit relatively weak, inhibitor of the essential HH pathway signal transducer SMO. As the effects of THC were dependent on a complementary, but insufficient, genetic deficiency, we categorize it as a 'conditional teratogen'. Cannabis consumption during pregnancy may therefore result in partial inhibition of a major morphogenetic pathway in embryos, thereby contributing to the complex combination of genetic and environmental risk factors that are thought to underlie many common developmental disorders.

THC inhibits HH signaling *in vitro* and *in vivo*

Eaton and colleagues first reported that endocannabinoids and phytocannabinoids inhibit HH signaling, but did not investigate cannabinoid effects in a vertebrate model *in vivo*, and did not focus on THC (Khaliullina et al., 2015). Our results are consistent with the conclusion that THC is a direct inhibitor of SMO. These findings

Development (2021) 148, dev199585. doi:10.1242/dev.199585

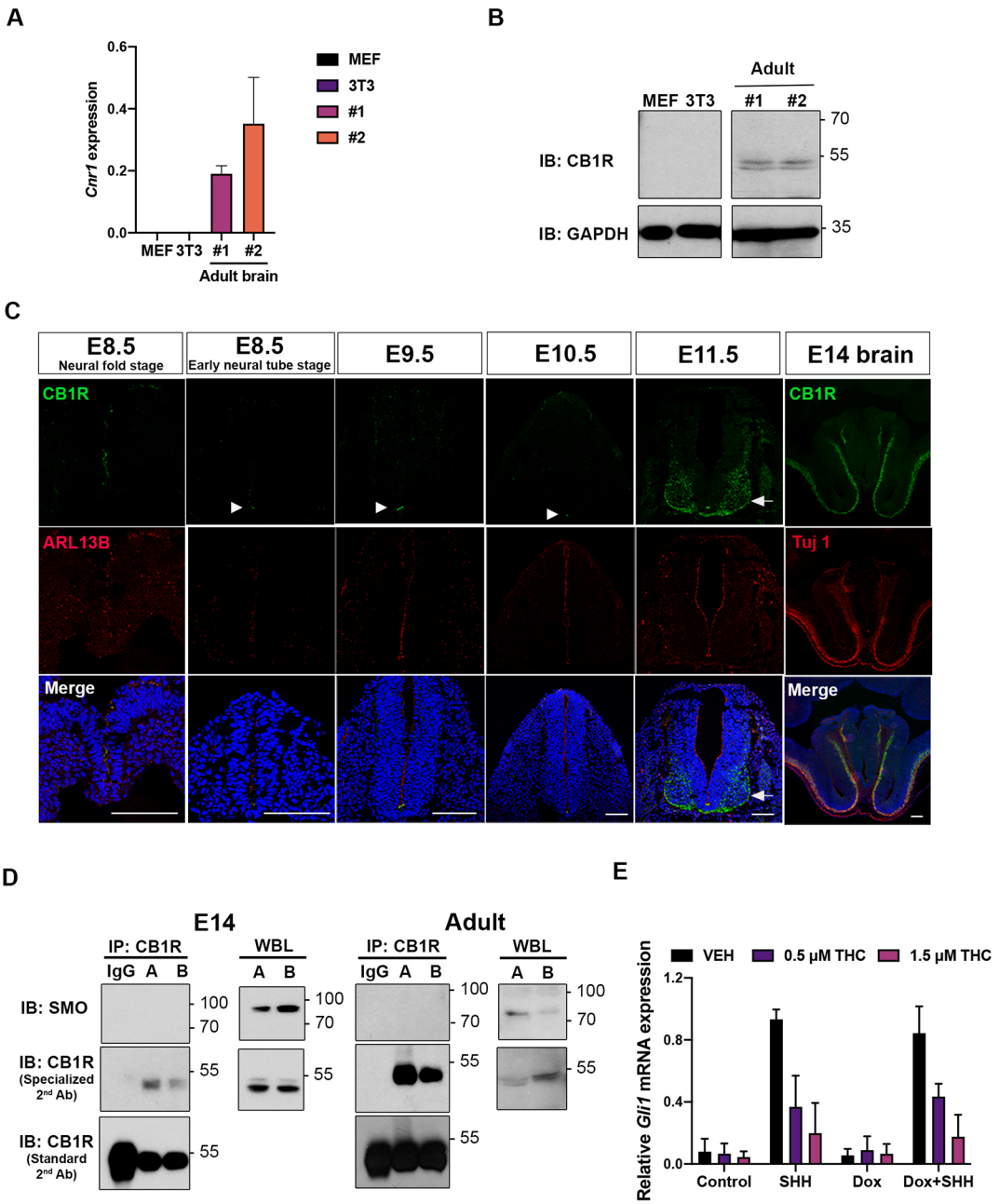

Fig. 6. CB1R is not required for THC-mediated inhibition of HH signaling. (A,B) Expression of *Cnr1* mRNA and CB1R protein in MEFs, NIH3T3 cells and adult mouse brain (two different samples) by qRT-PCR (A) and immunoblotting (B). Note that HH-responsive MEFs and NIH3T3 cells do not express *Cnr1*/CB1R. Number of PCR cycles: MEFs=30; 3T3=35; brain=21. (C) Forelimb level sections of mouse neural tubes at the indicated stages were stained with antibodies to CB1R and ARL13B and with DAPI (blue). Little to no CB1R is detected in the neural tube at E8.5, E9.5 or E10.5, except in a small number of cells in the ventricular zone of the floor plate (arrowheads). CB1R expression in the non-HH-responsive mantle zone at E11.5 is indicated by the arrow. ARL13B marks ciliated cells in the HH-responsive ventricular zone. CB1R staining of an E14 mouse brain section is used as a control, along with the neural differentiation marker, Tuj1 (red). Scale bars: 100 µm. (D) SMO does not co-immunoprecipitate (IP) with CB1R in lysates of E14 mouse brain or adult mouse brain (designated A and B for the two individual E14 and two individual adult samples, respectively). Whole-brain lysates (WBL) were directly immunoblotted (IB) as a control. Light chain-specific (GeneTex or Jackson ImmunoResearch) secondary antibody ('specialized 2nd Ab') was used to avoid detection of IgG heavy chain, which is of similar MW to CB1R (and seen in the blots using a 'Standard 2nd Ab'). The IgG lane is an IP with control, non-immune IgG in place of anti-CB1R antibody. (E) Exogenous expression of CB1R in NIH3T3 cells does not alter THC dose-dependent inhibition of SHH signaling, measured by induction of endogenous *Gli1* expression. Dox, cells pretreated with doxycycline to induce CB1R expression (see Fig. S4A). Values are mean±s.d., *n*=3.

include: (1) the inhibitory activity of THC mapped downstream of PTCH1 and upstream of SUFU; (2) THC prevented translocation of SMO to primary cilia upon pathway activation, without obviously altering cilia themselves; and (3) THC competed with a cyclopamine derivative for binding to SMO expressed on cells. THC therefore acted similarly to the well-studied SMO inhibitor SANT1, although it is much less potent than SANT1. The ability of THC to induce HH loss-of-function phenotypes in mice with a subthreshold HH signaling defect is fully consistent with its function as a relatively weak SMO inhibitor. In fact, THC treatment and *Shh* heterozygosity acted similarly in $Cdon^{-/-}$ mice, in that each enhanced the effects of *Cdon* mutation on facial midline and VNT

Development (2021) 148, dev199585. doi:10.1242/dev.199585

patterning, but neither was sufficient to perturb patterning on their own (Tenzen et al., 2006).

The THC structural analog CBD inhibited HH signaling *in vitro* with a similar IC50 as THC, but was much weaker at affecting SMO translocation to cilia and did not effectively compete for binding to SMO. CBD is therefore likely to inhibit HH signaling by a molecular mechanism somewhat distinct from that of THC, even if SMO might be its target. The SMO transmembrane domain has several potential binding modalities for small molecules (Kowatsch et al., 2019; Qi and Li, 2020), and it is possible that CBD binds in a deeper portion of the transmembrane pocket than cyclopamine, and so does not displace it. Such binding may induce a SMO conformation that does not efficiently block ciliary trafficking but inhibits adoption of an active conformation. Alternatively, CBD could bind to the amino-terminal cysteine-rich domain, displacing allosteric regulators (Huang et al., 2018). THC and CBD exert their effects outside the HH pathway via different receptors, so, despite being closely related, these compounds have important structural features that distinguish their activities (Dos Santos et al., 2021). The psychoactive properties of THC are the major reason people consume cannabis; these properties are not shared by CBD. However, CBD is available over the counter and viewed by many as generally beneficial, or at least innocuous, so it will be important to test CBD for conditional teratogenicity also.

While this work was in progress, Fish et al. reported studies on the effects of several phytocannabinoids and synthetic cannabinoids, including THC, in C57BL/6J mice (Fish et al., 2019). Consistent with the work reported here, THC induced 'minor alterations of pupil shape and size' in these mice, but exacerbated effects on eye morphology induced by fetal alcohol exposure (Fish et al., 2019).

CB1R is not required for THC to inhibit HH pathway signaling

It has been suggested that cannabinoids inhibit HH signaling via CB1R-SMO heterodimers (Fish et al., 2019). Evidence for this conclusion included co-immunoprecipitation of CB1R with SMO (Fish et al., 2019). However, our findings showed that CB1R is not required for THC to inhibit the HH pathway and argue against CB1R-SMO interaction. There are several lines of evidence for these conclusions. First, NIH3T3 cells and MEFs responded to HH signaling in a THC-inhibitable manner, yet they do not express detectable *Cnr1* mRNA or CB1R protein. Furthermore, THC inhibited VNT patterning, but VNT cells expressed little CB1R from E8.5 to E10.5, a period when they are acquiring neuronal identity in response to SHH signaling. This is consistent with mRNA *in situ* hybridization for *Cnr1* expression at a similar stage of the developing chick VNT (Watson et al., 2008). Second, we attempted to co-immunoprecipitate CB1R and SMO without success. The previously reported, co-precipitating band identified as CB1R in anti-SMO immunoprecipitates migrated at ∼100 kDa (Fish et al., 2019). The calculated molecular weight of CB1R is 53 kDa, approximately the size of the band we detected in our experiments. A recent study used multiple CB1R antibodies against brain lysates from control and *Cnr1* null mice (Esteban et al., 2020). All antibodies recognized a band of ∼53 kDa, that was specifically lost in the knockout mice. It is likely, therefore, that the ∼100 kDa band that co-immunoprecipitated with SMO was not CB1R. Third, exogenous expression of CB1R in NIH3T3 cells did not alter the dose dependency of THC-mediated inhibition of SHH signaling. Furthermore, CB1R did not localize to primary cilia in the presence or absence of THC, plus or minus SHH ligand. It was reported that the CB1R inhibitor SR141716A rescued eye phenotypes associated with *in utero* exposure of C57BL/6 mice to the synthetic cannabinoid CP55,940, or to CP55,940 plus alcohol (Fish et al., 2019). However, the eye phenotypes in this system are not distinctive to HH loss of function, and CB1R agonism may play a role in their genesis. Finally, although the role of endocannabinoids as inhibitors of vertebrate HH signaling is unknown, it is very unlikely that any such role would require CB1R or CB2R, as *Cnr1; Cnr2* double mutant mice are viable and do not display any reported HH gain-of-function phenotypes (Rowley et al., 2017; Sophocleous et al., 2017). This is in contrast to the strong gain-of-function phenotypes seen in embryos upon loss of established negative regulators of the HH pathway (e.g. *Ptch1*, *Sufu*, *Gnas*, *Gpr161*, *Ankmy2*) (Goodrich et al., 1997; Mukhopadhyay et al., 2013; Regard et al., 2013; Somatilaka et al., 2020; Svard et al., 2006).

Taken together, we conclude that CB1R is not required for THC to inhibit HH signaling. Although our findings do not conclusively rule out formation of CB1R-SMO complexes, neither our work nor published studies offer compelling evidence that such complexes exist.

THC as a potential risk factor in developmental disorders

The causes of common developmental disorders are often unknown. Many cases likely arise from a combination of subthreshold genetic and environmental insults, i.e. multifactorial etiology (Beames and Lipinski, 2020; Krauss and Hong, 2016). Whole-genome sequencing should eventually reveal a great majority of genetic contributions to such defects; subthreshold environmental risk factors, however, are more difficult to identify. The HH signaling pathway plays a fundamental role during development and is involved in growth and morphogenesis of a wide variety of body structures, including limbs, brain, heart and craniofacial structures (Petryk et al., 2015; Sagner and Briscoe, 2019; Tickle and Towers, 2017). Mutations in HH pathway components are involved in several developmental disorders, including Greig cephalopolysyndactyly syndrome, Gorlin syndrome, Brachydactyly A1 and HPE (Nieuwenhuis and Hui, 2005). Environmental agents that perturb HH signaling during specific times during embryogenesis may therefore be risk factors for developmental disorders, perhaps working in concert with predisposing genetic variants.

Cannabis is the most frequently used illicit drug during pregnancy and in young women of childbearing age; as legalization progresses, use will presumably increase. Furthermore, the THC concentration of both medicinal and recreational cannabis is currently very high (∼20% THC) (Cash et al., 2020). Identification of a potential role of cannabis consumption in the etiology of structural birth defects is significant, as it would represent an avoidable risk factor. Cannabinoids are HH pathway inhibitors but they have not been linked to human HPE, the most common outcome of genetic deficiency in HH signaling (Croen et al., 2000; Linn et al., 1983; Miller et al., 2010; van Gelder et al., 2009, 2010). HPE occurs in ∼1:250 conceptions, with >97% succumbing to intrauterine lethality (Leoncini et al., 2008; Shiota, 2021; Shiota and Yamada, 2010). Ordinarily, epidemiology would be used to assess whether specific environmental agents are risk factors, but epidemiological studies on possible teratogenic effects of cannabis have been neither designed nor powered to detect a link with HPE. There are several reasons for this. First, the >97% *in utero* lethality rate results in low case numbers that can be studied (Muenke and Beachy, 2001). Second, the window of sensitivity to teratogen-induced HPE in model systems is narrow and equivalent to the third week of human pregnancy (Heyne et al., 2015), a time when many women do not yet know they are pregnant. Such women may use cannabis at this stage, stop when they know they are pregnant, and self-report as not using the drug (Linn et al.,

Development (2021) 148, dev199585. doi:10.1242/dev.199585

1983). Finally, complex etiologies that involve subthreshold insults, as can occur with HPE, are often difficult to parse with epidemiology. Nevertheless, recent findings that correlate increased cannabis usage with specific structural birth defects (Reece and Hulse, 2019, 2020), combined with our identification of THC as a conditional teratogen, indicates that further research into this question is important and of significant public health relevance.

MATERIALS AND METHODS

Mice

All animal procedures were conducted in accordance with institutional guidelines for the care and use of laboratory animals as approved by the Institutional Animal Care and Use Committee (IACUC) of the Icahn School of Medicine at Mount Sinai. Two- to three-month-old *Cdon*$^{+/-}$ mice on a 129S6/SvEvTac (129S6) background (Cole and Krauss, 2003; Hong and Krauss, 2012) were mated for 1-2 h and plugged females were collected. The time of the plug was designated as E0.0. THC was injected intraperitoneally at selected times and various doses with 0.3% Tween-80 in saline as a vehicle. Offspring were examined as whole embryos at E14.0 for external signs of HPE. In other experiments, embryos were collected at various time points for analysis and staged for comparison by number of somites (see figure legends). Injected females were also assessed for plasma concentration of THC and metabolites over 60 h using a BIOO Scientific MaxSignal THC ELISA kit, according to the manufacturer's instructions. THC did not have obvious effects on embryo size at any stage.

Cannabinoids

THC and CBD were obtained from the NIDA Drug Supply Program. Δ9-THC (50 mg/ml in ethanol solution) was evaporated under nitrogen gas, dissolved in 0.9% NaCl (saline) containing 0.3% Tween 80 to a concentration of 0.75 mg/ml (DiNieri and Hurd, 2012) for administration to mice. THC and CBD were diluted to 0.75 mg/ml in ethanol solution for treatment of cells *in vitro*.

Whole-mount *in situ* hybridization

Whole-mount RNA *in situ* hybridization was performed according to standard protocols (Hong and Krauss, 2012). Briefly, E10 embryos were dissected out and fixed in 4% paraformaldehyde in PBS, dehydrated through a graded methanol series, and stored at −20°C. Rehydrated embryos were treated with 10 µg/ml proteinase K (Qiagen) in PBS, 0.1% Tween-20 (PBST) according to stage. Embryos were rinsed with PBST, post-fixed and hybridized with digoxygenin (DIG)-labeled probe in hybridization mix (50% formamide, 1.3× SSC pH 5.0, 5 mM EDTA, 50 µg/ml yeast tRNA, 100 µg/ml heparin, 0.2% Tween-20, 0.5% CHAPS) overnight at 65°C. They were washed, blocked with 2% Roche blocking reagent (Roche, 11096176001), 20% heat-inactivated lamb serum in Tris-buffered saline with 0.1% Tween-20 (TBST) and incubated with alkaline phosphate-conjugated anti-DIG antibody (Roche, 11093274910, 1:2000) in blocking buffer overnight at 4°C. After washing with TBST and NTMT (100 mM NaCl, 100 mM Tris pH 9.5, 50 mM $MgCl_2$ and 0.1% Tween-20), embryos were stained with BM Purple AP substrate (Roche) in the dark. Stained embryos were cleared in 80% glycerol and photographed with a Jenoptik ProgRes C3 camera attached to Nikon SMZ 1500 stereomicroscope. Captured images were assembled by Helicon Focus software (Helicon Soft).

Histology and immunohistochemistry

Embryos were fixed in 4% paraformaldehyde and embedded in paraffin for preparation of 7-µm-thick sections for H&E staining. Sections were then dehydrated through graded ethanol and xylene and mounted with Permount (Fisher Scientific). For VNT staining, embryos were infiltrated with sucrose and then embedded in O.C.T frozen medium. Cryosections (12 µm thick) of the forelimb region were collected and transferred to Superfrost Plus slides. After post-fixation in 4% paraformaldehyde, sections were washed three times in PBX (0.2% Triton X-100 in PBS). Primary and secondary antibodies were diluted in blocking buffer (1× PBX plus 3% BSA). Sections were incubated in primary antibodies overnight at 4°C. After washing with PBX, sections were incubated in secondary antibodies for 2 h at room temperature. The primary antibodies used were: OLIG2 (Millipore Sigma, AB9610, 1:1000), CB1R (Cayman Chemical, 10006590, 1:200), FOXA2 (Developmental Studies Hybridoma Bank, 4C7, 1:20), NKX2-2 (Developmental Studies Hybridoma Bank, 74.5A5, 1:20), ARL13B (NeuroMab, 75-287, 1:500), β-Tubulin III (Tuj1) (Millipore Sigma, T8660, 1:200). Secondary antibodies were: anti-rabbit Alexa 568 (Thermo Fisher Scientific, A-11011, 1:500) or Alexa 488 (Thermo Fisher Scientific, A-11008, 1:500); anti-mouse IgG1 Alexa 647 (Thermo Fisher Scientific, A-21240, 1:500); anti-mouse IgG2b Alexa 488 (Thermo Fisher Scientific, A-21141, 1:500); anti-mouse IgG2a Alexa 594 (Thermo Fisher Scientific, A-21135, 1:500). VECTASHIELD antifade mounting medium (Vector Laboratories, H-1000) was used to prevent signals from fading. Cryosections were imaged using a Leica SP5 DMI confocal microscope with a 20× objective. For VNT staining, five embryos of each group were analyzed. Between three and six individual sections per mouse were quantified for DAPI-, FOXA2-, NKX2-2- and OLIG2-positive cells. Data were processed using Fiji ImageJ software.

Plasmids

A mouse *Cnr1* cDNA fragment (Addgene, plasmid #13391) was cloned into an all-in-one tetracycline-inducible plasmid (pAS4.1w.Ppuro-aON, Academia Sinica, Taiwan). Recombinant lentivirus was produced by transfecting HEK293T cells with Lipofectamine 2000 (Invitrogen, 11668019) or TransIT-2020 transfection reagent (Mirus, MIR5404) and a third generation lentiviral package system, including pMD2.G, pRSV-Rev and pMDLg/RRE packaging plasmids (Dull et al., 1998). Recombinant lentivirus was used to infect NIH3T3 cells and stably expressing cells selected with 5 µg/ml puromycin (Thermo Fisher, A1113803). Conditional expression of CB1R was induced by the addition of doxycycline (Millipore Sigma, D9891).

Cell culture and qRT-PCR

NIH3T3 cells (obtained from Dr Stuart Aaronson, Icahn School of Medicine at Mount Sinai, New York, USA), HEK293T (obtained from ATCC), MEFs (freshly prepared), Neuro-2a cells (obtained from Dr Lakshmi Devi, Icahn School of Medicine at Mount Sinai, New York, USA), and *Ptch1*$^{-/-}$ and *Sufu*$^{-/-}$ MEFs (obtained from Dr Rune Toftgard, Karolinska Institute, Stockholm, Sweden) were grown in DMEM supplemented with 10% fetal bovine serum, penicillin and streptomycin (Thermo Fisher Scientific, 15140-122). All cells were free of contamination. For qRT-PCR, 80% confluent NIH3T3 cells or MEFs were cultured overnight in DMEM plus 2% FBS, after which they were incubated for another 24 h in fresh DMEM plus 2% fetal bovine serum supplemented with 5 ng/ml SHH (recombinant human amino terminal fragment of SHH, StemRD), SAG (Millipore Sigma, 566660) or cyclopamine (LC Laboratories, C-8770) in the presence or absence of antagonist. After incubation, total RNA was extracted using the RNeasy mini kit (Qiagen). For mouse E9 forebrain and E14 whole brain analyses, total RNA was extracted with the Trizol/RNeasy mini kit. Reverse transcription and cDNA production were performed with the Superscript III first strand synthesis system (Invitrogen). qPCR was performed using iQ SyBR Green Supermix (Bio-Rad) on an iCycler iQ5 (Bio-Rad). Gene expression levels were normalized to *Gapdh*. The primer sequences were as follows: *Gapdh*, AACGACCCCTTCATTGAC (forward primer) and TCCACGACATACTCAGCAC (reverse primer) (Dong et al., 2008); *Gli1*, CCAAGCCAACTTTATGTCAGGG (forward primer) and AGCCCGCTTCTTTGTTAATTTGA (reverse primer) (Harvard primer, 6754002a1); *Cnr1*, CTGGTTCTGATCCTGGTGGT (forward primer) and TGTCTCAGGTCCTTGCTCCT (reverse primer) (Ludányi et al., 2008); *Nkx2-1*, 5′-TCCAGCCTATCCCATCTGAACT-3′ (forward primer) and 5′- CAAGCGCATCTCACGTCTCA-3′ (reverse primer) (Zhang et al., 2007); *Ptch1*, 5′- AAAGAACTGCGGCAAGTTTTTG-3′ (forward primer) and 5′-CTTCTCCTATCTTCTGACGGGT-3′ (reverse primer) (Harvard primer, 6679519a1); *Shh*, 5′-CTGGCCAGATGTTTTCTGGT-3′ (forward primer) and 5′-GATGTCGGGGTTGTAATTGG-3′ (reverse primer) (Ochoa et al., 2010); *Bmp4*, 5′-GCTTCTGCAGGAACCAATGGA-3′ (forward primer) and 5′-TCCCGGTCTCAGGTATCAAACTAG-3′ (reverse primer) (Du et al., 2010).

Development (2021) 148, dev199585. doi:10.1242/dev.199585

Immunofluorescence and ciliary SMO localization measurement

Cells were plated on glass slides coated with rat tail collagen (Sigma-Aldrich, 11179179001). After incubation, cells were fixed in 4% paraformaldehyde at room temperature for 10 min and then in 100% methanol at −20°C for 4 min. Fixed cells were permeabilized in 0.1% Triton X-100 and blocked in 1× PBS plus 3% bovine serum albumin for 30 min. Cells were incubated in primary antibodies overnight at 4°C and then secondary antibodies for 2 h at room temperature. The primary antibodies used were: SMO (Santa Cruz Biotechnology, sc-166685, 1:50), ARL13B (Proteintech, 17711-1-AP, 1:500), γ-tubulin (Abcam, ab-11316, 1:200) and acetylated tubulin (Sigma-Aldrich, T7451, 1:500). Secondary antibodies used were: anti-rabbit Alexa 488; anti-mouse IgG1 Alexa 647; anti-mouse IgG2a Alexa 594 (Thermo Fisher, 1:500). Images were captured on a Leica SP5 DMI confocal microscope with a 63× oil objective. A shifted overlay of SMO and ARL13B signals was used for better visualization. For quantification of ciliary SMO, first a mask was determined by using the ARL13B image, and then the mask was applied to the corresponding SMO image where the fluorescence intensity was measured. An identical area nearby but outside the cilia was also measured to determine background fluorescence. Background subtraction was applied on each primary cilium. The percentage of ciliary SMO was determined by fluorescence intensity. Compared with the mean value of positive controls, when treatments decreased SMO signal by more than 50%, cilia were considered negative. The lengths of primary cilia were measured by the ARL13B signal. Between 100 and 140 cilia were analyzed per condition. Data were quantified using Fiji ImageJ software.

Immunoprecipitation

To detect the interaction of CB1R and SMO, mouse brain lysates were harvested in lysis buffer containing 50 mM Tris-HCl (pH 8.0), 150 mM NaCl, 2 mM EDTA, 10% glycerol, 0.5% Nonidet P40, 5 mM NaF, 1 mM Na_3VO_4, and a protease inhibitor cocktail (Sigma-Aldrich). Whole brain lysate was precleared with Protein G agarose (Roche, 11243233001) and the supernatant was immunoprecipitated with CB1R antibody overnight at 4°C. The lysate was then incubated with Protein G agarose for 3 h at 4°C. Material pulled down was washed with lysis buffer three times and eluted by boiling. Eluates were separated by SDS-PAGE and transferred to PVDF membranes, which were immunoblotted with primary antibodies against CB1R and SMO overnight at 4°C. Secondary antibodies used for western blotting were: anti-mouse (Cell Signaling Technology, 7076, 1:5000), HRP-conjugated anti-rabbit (Cell Signaling Technology, 7074, 1:5000) or HRP-conjugated anti-rabbit secondary antibodies, light chain specific (Genetex, GTX221666, 1:2000; Jackson ImmunoResearch, 211-032-171, 1:5000), which do not detect IgG heavy chain.

BODIPY-cyclopamine binding assays

BODIPY-CPA assays were carried out as detailed by Chen et al.(2002) with minor modifications. Briefly, SMO tagged at its C terminus with Myc epitope was expressed in 293T cells by transient transfection. Empty vector was transfected as a control. Twenty-four hours later, cells were plated on rat tail collagen-coated glass slides, and 24 h after that were incubated for 4 h in OPTI-MEM with 5 nM BODIPY-CPA (BioVision, 2160-50), in the presence or absence of competitor drug SANT1 (Millipore Sigma, 559303) or KAAD-cyclopamine (Calbiochem, 239804) at 37°C. The cells were washed with PBS and fixed in 4% paraformaldehyde for 15 min, followed by permeabilization with PBS containing 0.1% Triton X-100. SMO was detected with Myc antibody (Santa Cruz Biotechnology, sc-40, 1:500) and Alexa 568-conjugated mouse secondary antibody (Thermo Fisher, A-11011, 1:500). The cells were then imaged on a Leica DM5500 B upright microscope, capturing ten fields of view from each of three experiments, with the mean intensity from the ten fields/experiment plotted as data points in Fig. 5B. Representative fields are shown. Cells not expressing SMO-Myc or not incubated with BODIPY-CPA were used for background subtraction for both BODIPY and Alexa 568 channels. Data are presented as background-subtracted BODIPY intensity and Alexa 568 intensity for SMO-Myc-expressing cells.

Statistical analysis

Experiments were performed at least three independent times. Data were analyzed with GraphPad Prism 8. Graphs show mean values and error bars indicate s.d. Statistical analysis of the data was performed using two-tailed unpaired Student's *t*-test, ordinary one-way ANOVA with Tukey's multiple comparison test, or two-tailed Fischer's exact test as noted. Statistical significance was classified as $*P<0.05$, $**P<0.01$ or $***P<0.001$. A P-value of <0.05 was considered statistically significant.

Acknowledgements

The authors dedicate this paper to the memory of Suzanne Eaton. We thank Rune Toftgard for providing *Ptch1*$^{-/-}$ and *Sufu*$^{-/-}$ MEFs, Lakshmi Devi for providing Neuro-2a cells, Hungwen Chen for expression vectors, and Paul Wassarman and Phil Soriano for critical comments on the manuscript.

Competing interests

The authors declare no competing or financial interests.

Author contributions

Conceptualization: H.-F.L., R.S.K.; Methodology: H.-F.L., M.H., H.S.; Formal analysis: H.-F.L., M.H.; Investigation: H.-F.L., M.H.; Writing - original draft: H.-F.L., R.S.K.; Writing - review & editing: H.-F.L., M.H., H.S., Y.L.H., R.S.K.; Visualization: H.-F.L., M.H.; Supervision: Y.L.H., R.S.K.; Project administration: R.S.K.; Funding acquisition: Y.L.H., R.S.K.

Funding

This work was supported by a pilot grant from the Mindich Child Health and Development Institute, Icahn School of Medicine at Mount Sinai, NY, USA, grants from the National Institute on Drug Abuse (DA045971 to R.S.K, DA030359 to Y.L.H.), and the Tisch Cancer Institute at Mount Sinai (P30 CA196521 – Cancer Center Support Grant). Deposited in PMC for release after 12 months.

Peer review history

The peer review history is available online at https://journals.biologists.com/dev/article-lookup/doi/10.1242/dev.199585

References

Allen, B. L., Song, J. Y., Izzi, L., Althaus, I. W., Kang, J.-S., Charron, F., Krauss, R. S. and McMahon, A. P. (2011). Overlapping roles and collective requirement for the co-receptors GAS1, CDO and BOC in SHH pathway function. *Dev. Cell* **20**, 775-787. doi:10.1016/j.devcel.2011.04.018

Amberger, J. S., Bocchini, C. A., Scott, A. F. and Hamosh, A. (2019). OMIM.org: leveraging knowledge across phenotype-gene relationships. *Nucleic Acids Res.* **47**, D1038-D1043. doi:10.1093/nar/gky1151

Bangs, F. and Anderson, K. V. (2017). Primary cilia and mammalian Hedgehog signaling. *Cold Spring Harb Perspect Biol* **9**, a028175. doi:10.1101/cshperspect.a028175

Beames, T. G. and Lipinski, R. J. (2020). Gene-environment interactions: aligning birth defects research with complex etiology. *Development* **147**, dev191064. doi:10.1242/dev.191064

Cash, M. C., Cunnane, K., Fan, C. and Romero-Sandoval, E. A. (2020). Mapping cannabis potency in medical and recreational programs in the United States. *PLoS One* **15**, e0230167. doi:10.1371/journal.pone.0230167

Chen, J. K., Taipale, J., Cooper, M. K. and Beachy, P. A. (2002). Inhibition of Hedgehog signaling by direct binding of cyclopamine to Smoothened. *Genes & Dev* **16**, 2743-2748. doi:10.1101/gad.1025302

Christianson, A., Howson, C. P. and Modell, B. (2006). Global report on birth defects. In *March of Dimes Global Report on Birth Defects: The hidden toll of dying and disabled children*. White Plains, New York: March of Dimes Birth Defects Foundation, https://www.marchofdimes.org/materials/global-report-on-birth-defects-the-hidden-toll-of-dying-and-disabled-children-full-report.pdf.

Cohen, M. M.Jr. (2006). Holoprosencephaly: clinical, anatomic, and molecular dimensions. *Birth Defects Res Part A Clin Mol Teratol* **76**, 658-673. doi:10.1002/bdra.20295

Cole, F. and Krauss, R. S. (2003). Microform holoprosencephaly in mice that lack the Ig superfamily member Cdon. *Curr. Biol.* **13**, 411-415. doi:10.1016/S0960-9822(03)00088-5

Croen, L. A., Shaw, G. M. and Lammer, E. J. (2000). Risk factors for cytogenetically normal holoprosencephaly in California: a population-based case-control study. *Am. J. Med. Genet.* **90**, 320-325.

Dessaud, E., McMahon, A. P. and Briscoe, J. (2008). Pattern formation in the vertebrate neural tube: a sonic hedgehog morphogen-regulated transcriptional network. *Development* **135**, 2489-2503. doi:10.1242/dev.009324

DiNieri, J. and Hurd, Y. (2012). Rat Models of Prenatal and Adolescent Cannabis Exposure. In *Psychiatric Disorders Methods in Molecular Biology* (ed. F.H. Kobeissy), pp. 231-242. Humana Press.
Dong, J., Sulik, K. K. and Chen, S. Y. (2008). Nrf2-Mediated Transcriptional Induction of Antioxidant Response in Mouse Embryos Exposed to Ethanol in vivo: Implications for the Prevention of Fetal Alcohol Spectrum Disorders. *Antioxid Redox Signal.* **10**, 2023-2033.
Dos Santos, R. G., Hallak, J. E. C. and Crippa, J. A. S. (2021). Neuropharmacological Effects of the Main Phytocannabinoids: a narrative review. *Adv. Exp. Med. Biol.* **1264**, 29-45. doi:10.1007/978-3-030-57369-0_3
Du, J., Takeuchi, H., Leonhard-Melief, C., Shroyer, K. R., Dlugosz, M., Haltiwanger, R. S. and Holdener, B. C. (2010). O-fucosylation of thrombospondin type 1 repeats restricts epithelial to mesenchymal transition (EMT) and maintains epiblast pluripotency during mouse gastrulation. *Dev. Biol.* **346**, 25-38. doi:10.1016/j.ydbio.2010.07.008
Dubourg, C., Kim, A., Watrin, E., de Tayrac, M., Odent, S., David, V. and Dupé, V. (2018). Recent advances in understanding inheritance of holoprosencephaly. *Am. J. Med. Genet.* **178**, 258-269. doi:10.1002/ajmg.c.31619
Dull, T., Zufferey, R., Kelly, M., Mandel, R. J., Nguyen, M., Trono, D. and Naldini, L. (1998). A third-generation lentivirus vector with a conditional packaging system. *J. Virol.* **72**, 8463-8471. doi:10.1128/JVI.72.11.8463-8471.1998
Esteban, P. F., Garcia-Ovejero, D., Paniagua-Torija, B., Moreno-Luna, R., Arredondo, L. F., Zimmer, A., Martín, Á. A. and Molina-Holgado, E. (2020). Revisiting CB1 cannabinoid receptor detection and the exploration of its interacting partners. *J. Neurosci. Methods* **337**, 108680. doi:10.1016/j.jneumeth.2020.108680
Fish, E. W., Murdaugh, L. B., Zhang, C., Boschen, K. E., Boa-Amponsem, O., Mendoza-Romero, H. N., Tarpley, M., Chdid, L., Mukhopadhyay, S., Cole, G. J. et al. (2019). Cannabinoids exacerbate alcohol teratogenesis by a CB1-Hedgehog interaction. *Sci. Rep.* **9**, 16057. doi:10.1038/s41598-019-52336-w
Fraser, F. C. (1980). The William Allan Memorial Award Address: evolution of a palatable multifactorial threshold model. *Am. J. Hum. Genet.* **32**, 796-813.
Gigante, E. D. and Caspary, T. (2020). Signaling in the primary cilium through the lens of the Hedgehog pathway. *WIREs Dev Biol* **9**, e377. doi:10.1002/wdev.377
Gilbert, M. T., Sulik, K. K., Fish, E. W., Baker, L. K., Dehart, D. B. and Parnell, S. E. (2015). Dose-dependent teratogenicity of the synthetic cannabinoid CP-55,940 in mice. *Neurotoxicol. Teratol.* **58**, 15-22. doi:10.1016/j.ntt.2015.12.004
Gilbert-Barness, E. (2010). Teratogenic causes of malformations. *Ann. Clin. Lab. Sci.* **40**, 99-114.
Goodrich, L. V., Milenković, L., Higgins, K. M. and Scott, M. P. (1997). Altered neural cell fates and medulloblastoma in mouse patched mutants. *Science* **277**, 1109-1113.
Graham, E. S., Ball, N., Scotter, E. L., Narayan, P., Dragunow, M. and Glass, M. (2006). Induction of Krox-24 by endogenous cannabinoid type 1 receptors in Neuro2A cells is mediated by the MEK-ERK MAPK pathway and is suppressed by the phosphatidylinositol 3-kinase pathway. *J. Biol. Chem.* **281**, 29085-29095. doi:10.1074/jbc.M602516200
Grotenhermen, F. (2003). Pharmacokinetics and pharmacodynamics of cannabinoids. *Clin. Pharmacokinet.* **42**, 327-360. doi:10.2165/00003088-200342040-00003
Gunn, J. K. L., Rosales, C. B., Center, K. E., Nuñez, A., Gibson, S. J., Christ, C. and Ehiri, J. E. (2016). Prenatal exposure to cannabis and maternal and child health outcomes: a systematic review and meta-analysis. *BMJ Open* **6**, e009986. doi:10.1136/bmjopen-2015-009986
He, J. C., Gomes, I., Nguyen, T., Jayaram, G., Ram, P. T., Devi, L. A. and Iyengar, R. (2005). The G alpha(o/i)-coupled cannabinoid receptor-mediated neurite outgrowth involves Rap regulation of Src and Stat3. *J. Biol. Chem.* **280**, 33426-33434. doi:10.1074/jbc.M502812200
Heyne, G. W., Melberg, C. G., Doroodchi, P., Parins, K. F., Kietzman, H. W., Everson, J. L., Ansen-Wilson, L. J. and Lipinski, R. J. (2015). Definition of critical periods for hedgehog pathway antagonist-induced holoprosencephaly, cleft lip, and cleft palate. *PLoS One* **10**, e0120517.
Hong, M. and Krauss, R. S. (2012). *Cdon* mutation and fetal ethanol exposure synergize to produce midline signaling defects and holoprosencephaly spectrum disorders in mice. *PLoS Genet.* **8**, e1002999.
Hong, M. and Krauss, R. S. (2018). Modeling the complex etiology of holoprosencephaly in mice. *Am J of Med Genet* **178C**, 140-150. doi:10.1002/ajmg.c.31611
Huang, P., Nedelcu, D., Watanabe, M., Jao, C., Kim, Y., Liu, J. H. and Salic, A. (2016). Cellular cholesterol directly activates smoothened in Hedgehog signaling. *Cell* **166**, 1176-1187.e1114. doi:10.1016/j.cell.2016.08.003
Huang, P., Zheng, S., Wierbowski, B. M., Kim, Y., Nedelcu, D., Aravena, L., Liu, J., Kruse, A. C. and Salic, A. (2018). Structural basis of smoothened activation in Hedgehog signaling. *Cell* **174**, 312-324.e316. doi:10.1016/j.cell.2018.04.029
Izzi, L., Lévesque, M., Morin, S., Laniel, D., Wilkes, B. C., Mille, F., Krauss, R. S., McMahon, A. P., Allen, B. L. and Charron, F. (2011). Boc and Gas1 each form distinct Shh receptor complexes with Ptch1 and are required for Shh-mediated cell proliferation. *Dev. Cell* **20**, 788-801. doi:10.1016/j.devcel.2011.04.017
Khaliullina, H., Bilgin, M., Sampaio, J. L., Shevchenko, A. and Eaton, S. (2015). Endocannabinoids are conserved inhibitors of the Hedgehog pathway. *Proc Natl Acad Sci. USA* **112**, 3415-3420. doi:10.1073/pnas.1416463112
Kong, J. H., Siebold, C. and Rohatgi, R. (2019). Biochemical mechanisms of vertebrate hedgehog signaling. *Development* **146**, dev166892. doi:10.1242/dev.166892
Kowatsch, C., Woolley, R. E., Kinnebrew, M., Rohatgi, R. and Siebold, C. (2019). Structures of vertebrate Patched and Smoothened reveal intimate links between cholesterol and Hedgehog signalling. *Curr. Opin. Struct. Biol.* **57**, 204-214. doi:10.1016/j.sbi.2019.05.015
Krauss, R. S. (2007). Holoprosencephaly: new models, new insights. *Expert Rev. Mol. Med.* **9**, 1-17. doi:10.1017/S1462399407000440
Krauss, R. S. and Hong, M. (2016). Gene–environment Interactions and the etiology of birth defects. *Curr. Top. Dev. Biol.* **116**, 569-580. doi:10.1016/bs.ctdb.2015.12.010
Lee, R. T. H., Zhao, Z. and Ingham, P. W. (2016). Hedgehog signalling. *Development* **143**, 367-372. doi:10.1242/dev.120154
Leoncini, E., Baranello, G., Orioli, I. M., Annerén, G., Bakker, M., Bianchi, F., Bower, C., Canfield, M. A., Castilla, E. E., Cocchi, G. et al. (2008). Frequency of holoprosencephaly in the International Clearinghouse Birth Defects Surveillance Systems: searching for population variations. *Birth Defects Res. A Clin. Mol. Teratol* **82**, 585-591. doi:10.1002/bdra.20479
Linn, S., Schoenbaum, S. C., Monson, R. R., Rosner, R., Stubblefield, P. C. and Ryan, K. J. (1983). The association of marijuana use with outcome of pregnancy. *Am. J. Public Health* **73**, 1161-1164. doi:10.2105/AJPH.73.10.1161
Lovely, C., Rampersad, M., Fernandes, Y. and Eberhart, J. K. (2017). Gene–environment interactions in development and disease. *WIREs Dev Biol* **6**, e247. doi:10.1002/wdev.247
Lu, H. C. and Mackie, K. (2020). Review of the Endocannabinoid System. *Biol Psychiatry Cogn Neurosci Neuroimaging* **6**, 607-615. doi:10.1016/j.bpsc.2020.07.016
Ludányi, A., Eross, L., Czirják, S., Vajda, J., Halász, P., Watanabe, M., Palkovits, M., Maglóczky, Z., Freund, T. F. and Katona, I. (2008). Downregulation of the CB1 cannabinoid receptor and related molecular elements of the endocannabinoid system in epileptic human hippocampus. *J. Neurosci.* **28**, 2976-2990. doi:10.1523/JNEUROSCI.4465-07.2008
Maccarrone, M., Bab, I., Bíró, T., Cabral, G. A., Dey, S. K., Di Marzo, V., Konje, J. C., Kunos, G., Mechoulam, R., Pacher, P. et al. (2015). Endocannabinoid signaling at the periphery: 50 years after THC. *Trends Pharmacol. Sci.* **36**, 277-296. doi:10.1016/j.tips.2015.02.008
Miller, E. A., Rasmussen, S. A., Siega-Riz, A. M., Frías, J. L., Honein, M. A. and Study, N. B. D. P. (2010). Risk factors for non-syndromic holoprosencephaly in the National Birth Defects Prevention Study. *Am. J. Med. Genet. C Semin. Med. Genet.* **154C**, 62-72.
Muenke, M. and Beachy, P. A. (2001). Holoprosencephaly. In *The Metabolic & Molecular Bases of Inherited Disease* (ed. C.R. Scriver, A.L. Beaudet, W.S. Sly and D. Valle), pp. 6203-6230. New York: McGraw-Hill.
Mukhopadhyay, S., Wen, X., Ratti, N., Loktev, A., Rangell, L., Scales, S. J. and Jackson, P. K. (2013). The ciliary G-Protein-coupled receptor Gpr161 negatively regulates the sonic Hedgehog pathway via cAMP signaling. *Cell* **152**, 210-223. doi:10.1016/j.cell.2012.12.026
Mulder, J., Aguado, T., Keimpema, E., Barabás, K., Rosado, C. J. B., Nguyen, L., Monory, K., Marsicano, G., Di Marzo, V., Hurd, Y. L. et al. (2008). Endocannabinoid signaling controls pyramidal cell specification and long-range axon patterning. *Proc Natl Acad Sci* **105**, 8760-8765.
Nieuwenhuis, E. and Hui, C.-C. (2005). Hedgehog signaling and congenital malformations. *Clin. Genet.* **67**, 193-208. doi:10.1111/j.1399-0004.2004.00360.x
Ochoa, B., Syn, W.-K., Delgado, I., Karaca, G. F., Jung, Y., Wang, J., Zubiaga, A. M., Fresnedo, O., Omenetti, A., Zdanowicz, M. et al. (2010). Hedgehog signaling is critical for normal liver regeneration after partial hepatectomy in mice. *Hepatology* **51**, 1712-1723. doi:10.1002/hep.23525
Petrov, K., Wierbowski, B. M. and Salic, A. (2017). Sending and receiving Hedgehog signals. *Annu. Rev. Cell Dev. Biol.* **33**, 145-168. doi:10.1146/annurev-cellbio-100616-060847
Petryk, A., Graf, D. and Marcucio, R. (2015). Holoprosencephaly: signaling interactions between the brain and the face, the environment and the genes, and the phenotypic variability in animal models and humans. *Wiley Interdiscip Rev Dev Biol* **4**, 17-32. doi:10.1002/wdev.161
Psychoyos, D., Vinod, K. Y., Cao, J., Xie, S., Hyson, R. L., Wlodarczyk, B., He, W., Cooper, T. B., Hungund, B. L. and Finnell, R. H. (2012). Cannabinoid receptor 1 signaling in embryo neurodevelopment. *Birth Defects Res. B Dev. Reprod. Toxicol.* **95**, 137-150. doi:10.1002/bdrb.20348
Qi, X. and Li, X. (2020). Mechanistic insights into the generation and transduction of Hedgehog signaling. *Trends Biochem. Sci.* **45**, 397-410. doi:10.1016/j.tibs.2020.01.006
Radhakrishnan, A., Rohatgi, R. and Siebold, C. (2020). Cholesterol access in cellular membranes controls Hedgehog signaling. *Nat. Chem. Biol.* **16**, 1303-1313. doi:10.1038/s41589-020-00678-2
Reece, A. S. and Hulse, G. K. (2019). Cannabis teratology explains current patterns of Coloradan congenital defects: the contribution of increased Cannabinoid

exposure to rising teratological trends. *Clinical Pediatrics* **58**, 1085-1123. doi:10.1177/0009922819861281

Reece, A. S. and Hulse, G. K. (2020). Contemporary epidemiology of rising atrial septal defect trends across USA 1991–2016: a combined ecological geospatiotemporal and causal inferential study. *BMC Pediatr.* **20**, 539. doi:10.1186/s12887-020-02431-z

Regard, J. B., Malhotra, D., Gvozdenovic-Jeremic, J., Josey, M., Chen, M., Weinstein, L. S., Lu, J., Shore, E. M., Kaplan, F. S. and Yang, Y. (2013). Activation of Hedgehog signaling by loss of GNAS causes heterotopic ossification. *Nat. Med.* **19**, 1505-1512. doi:10.1038/nm.3314

Ribes, V., Balaskas, N., Sasai, N., Cruz, C., Dessaud, E., Cayuso, J., Tozer, S., Yang, L. L., Novitch, B., Marti, E. et al. (2010). Distinct Sonic Hedgehog signaling dynamics specify floor plate and ventral neuronal progenitors in the vertebrate neural tube. *Genes Dev.* **24**, 1186-1200. doi:10.1101/gad.559910

Roessler, E., Vélez, J. I., Zhou, N. and Muenke, M. (2012). Utilizing prospective sequence analysis of SHH, ZIC2, SIX3 and TGIF in holoprosencephaly probands to describe the parameters limiting the observed frequency of mutant gene×gene interactions. *Mol. Genet. Metab.* **105**, 658-664. doi:10.1016/j.ymgme.2012.01.005

Roessler, E., Hu, P. and Muenke, M. (2018). Holoprosencephaly in the genomics era. *Am J Med Genet Part C* **178**, 165-174. doi:10.1002/ajmg.c.31615

Rohatgi, R., Milenkovic, L., Corcoran, R. B. and Scott, M. P. (2009). Hedgehog signal transduction by Smoothened: Pharmacologic evidence for a 2-step activation process. *Proc Natl Acad Sci* **106**, 3196-3201.

Rowley, S., Sun, X., Lima, I. V., Tavenier, A., de Oliveira, A. C. P., Dey, S. K. and Danzer, S. C. (2017). Cannabinoid receptor 1/2 double-knockout mice develop epilepsy. *Epilepsia* **58**, e162-e166. doi:10.1111/epi.13930

Sagner, A. and Briscoe, J. (2019). Establishing neuronal diversity in the spinal cord: a time and a place. *Development* **146**, dev182154. doi:10.1242/dev.182154

Schurman, L. D., Lu, D., Kendall, D. A., Howlett, A. C. and Lichtman, A. H. (2020). Molecular mechanism and Cannabinoid pharmacology. *Handb. Exp. Pharmacol.* **258**, 323-353. doi:10.1007/164_2019_298

Sever, N., Mann, R. K., Xu, L., Snell, W. J., Hernandez-Lara, C. I., Porter, N. A. and Beachy, P. A. (2016). Endogenous B-ring oxysterols inhibit the Hedgehog component Smoothened in a manner distinct from cyclopamine or side-chain oxysterols. *Proc. Natl. Acad. Sci. U.S.A.* **113**, 5904-5909. doi:10.1073/pnas.1604984113

Sharpe, H. J., Wang, W., Hannoush, R. N. and de Sauvage, F. J. (2015). Regulation of the oncoprotein Smoothened by small molecules. *Nat. Chem. Biol.* **11**, 246-255. doi:10.1038/nchembio.1776

Shiota, K. (2021). A life-table analysis of the intrauterine fate of malformed human embryos and fetuses. *Birth Defects Res* **113**, 623-632. doi:10.1002/bdr2.1888

Shiota, K. and Yamada, S. (2010). Early pathogenesis of holoprosencephaly. *Am. J. Med. Genet. C Semin. Med. Genet.* **154C**, 22-28.

Somatilaka, B. N., Hwang, S.-H., Palicharla, V. R., White, K. A., Badgandi, H., Shelton, J. M. and Mukhopadhyay, S. (2020). Ankmy2 prevents smoothened-independent hyperactivation of the Hedgehog pathway via cilia-regulated adenylyl cyclase signaling. *Dev. Cell* **54**, 710-726.e718. doi:10.1016/j.devcel.2020.06.034

Sophocleous, A., Marino, S., Kabir, D., Ralston, S. H. and Idris, A. I. (2017). Combined deficiency of the Cnr1 and Cnr2 receptors protects against age-related bone loss by osteoclast inhibition. *Aging Cell* **16**, 1051-1061. doi:10.1111/acel.12638

Svard, J., Heby-Henricson, K., Persson-Lek, M., Rozell, B., Lauth, M., Bergstrom, A., Ericson, J., Toftgard, R. and Teglund, S. (2006). Genetic elimination of suppressor of fused reveals an essential repressor function in the mammalian Hedgehog signaling pathway. *Dev. Cell* **10**, 187-197. doi:10.1016/j.devcel.2005.12.013

Taipale, J., Chen, J. K., Cooper, M. K., Wang, B., Mann, R. K., Milenkovic, L., Scott, M. P. and Beachy, P. A. (2000). Effects of oncogenic mutations in *Smoothened* and *Patched* can be reversed by cyclopamine. *Nature* **406**, 1005-1009.

Tenzen, T., Allen, B. L., Cole, F., Kang, J.-S., Krauss, R. S. and McMahon, A. P. (2006). The cell surface membrane proteins Cdo and Boc are components and targets of the hedgehog signaling pathway and feedback network in mice. *Dev. Cell* **10**, 647-656. doi:10.1016/j.devcel.2006.04.004

Tickle, C. and Towers, M. (2017). Sonic Hedgehog Signaling in limb development. *Front Cell Dev Biol* **5**, 14. doi:10.3389/fcell.2017.00014

van Gelder, M. M., Reefhuis, J., Caton, A. R., Werler, M. M., Druschel, C. M. and Roeleveld, N. and **the National Birth Defects Prevention Study** (2009). Maternal periconceptional illicit drug use and the risk of congenital malformations. *Epidemiology* **20**, 60-66. doi:10.1097/EDE.0b013e31818e5930

van Gelder, M. M. H. J., Reefhuis, J., Caton, A. R., Werler, M. M., Druschel, C. M. and Roeleveld, N. (2010). Characteristics of pregnant illicit drug users and associations between cannabis use and perinatal outcome in a population-based study. *Drug and Alcohol Depend* **109**, 243-247. doi:10.1016/j.drugalcdep.2010.01.007

Volkow, N. D., Compton, W. M. and Wargo, E. M. (2017). The risks of Marijuana use during pregnancy. *JAMA* **317**, 129-130. doi:10.1001/jama.2016.18612

Wallingford, J. B. (2019). We are all developmental biologists. *Dev. Cell* **50**, 132-137. doi:10.1016/j.devcel.2019.07.006

Watson, S., Chambers, D., Hobbs, C., Doherty, P. and Graham, A. (2008). The endocannabinoid receptor, CB1, is required for normal axonal growth and fasciculation. *Mol Cellular Neurosci* **38**, 89-97. doi:10.1016/j.mcn.2008.02.001

Webber, D. M., MacLeod, S. L., Bamshad, M. J., Shaw, G. M., Finnell, R. H., Shete, S. S., Witte, J. S., Erickson, S. W., Murphy, L. D. and Hobbs, C. (2015). Developments in our understanding of the genetic basis of birth defects. *Birth Defects Research Part A: Clinical and Molecular Teratology* **103**, 680-691.

Wierbowski, B. M., Petrov, K., Aravena, L., Gu, G., Xu, Y. and Salic, A. (2020). Hedgehog pathway activation requires coreceptor-catalyzed, lipid-dependent relay of the Sonic Hedgehog ligand. *Dev. Cell* **55**, 450-467.e458. doi:10.1016/j.devcel.2020.09.017

Wilson, C. W., Chen, M.-H. and Chuang, P.-T. (2009). Smoothened adopts multiple active and inactive conformations capable of trafficking to the primary cilium. *PLoS One* **4**, e5182. doi:10.1371/journal.pone.0005182

Young-Wolff, K. C., Tucker, L.-Y., Alexeeff, S., Armstrong, M., Conway, A., Weisner, C. and Goler, N. (2017). Trends in self-reported and biochemically tested Marijuana use among pregnant females in California from 2009-2016. *JAMA* **318**, 2490-2491. doi:10.1001/jama.2017.17225

Zhang, Y., Rath, N., Hannenhalli, S., Wang, Z., Cappola, T., Kimura, S., Atochina-Vasserman, E., Lu, M. M., Beers, M. F. and Morrisey, E. E. (2007). GATA and Nkx factors synergistically regulate tissue-specific gene expression and development in vivo. *Development* **134**, 189-198. doi:10.1242/dev.02720

Zhang, W., Hong, M., Bae, G.-U., Kang, J.-S. and Krauss, R. S. (2011). *Boc* modifies the holoprosencephaly spectrum of *Cdo* mutant mice. *Dis Model Mech* **4**, 368-380.

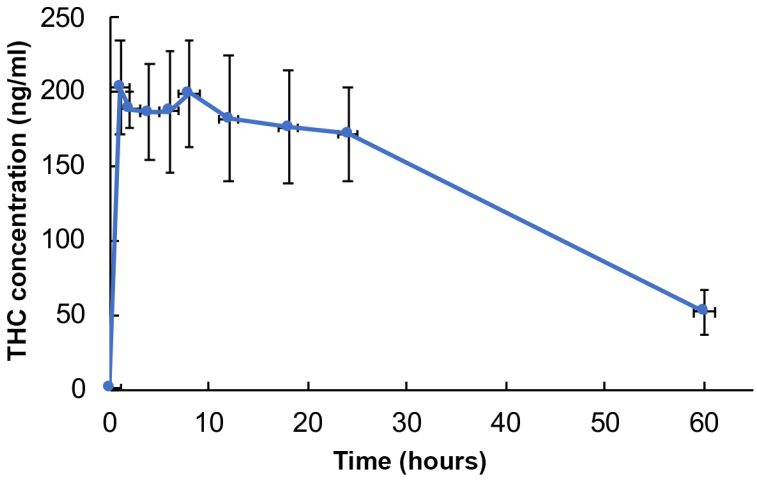

Fig. S1. Maternal blood THC levels.

The level of THC plus THC metabolites (11-hydroxy-THC and 11-nor-9-carboxy-THC) was measured over a 60-hour time course after IP administration of 15 mg/kg THC. Serum was collected and analyzed by ELISA. Values are means ± SD, N=4-10 mice per time point.

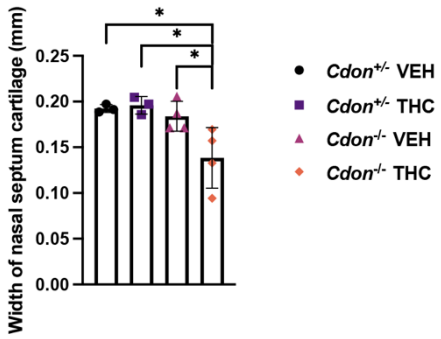

Fig. S2. Reduced width of the nasal septum cartilage in THC-treated *Cdon*$^{-/-}$ embryos.

The width of nasal septum of embryos was quantified by measuring the widest point in H&E sections taken at level A" in Figure 1. Three or four serial sections per embryo at this level were measured and each point represents the mean ± SD, N=3-4 embryos. Pregnant females were administered 15 mg/kg THC or VEH at E7.5 and analyzed at E14. *, $p<0.05$ with ordinary one-way ANOVA with Tukey's multiple comparison test.

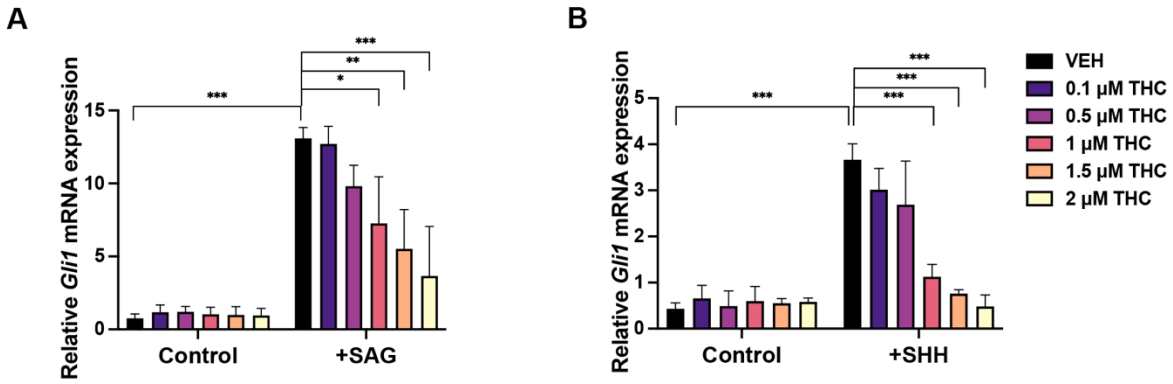

Fig. S3. THC suppresses SHH-induced *Gli1* expression in MEFs.

A. NIH3T3 cells were treated with 50 nM SAG and the indicated concentrations of THC for 24 hr.

B. MEFs were treated with 5 ng/ml SHH and the indicated concentrations of THC for 24 hr. Relative *Gli1* mRNA expression was analyzed by qRT-PCR. Values are means ± SD, N=3. *, **, ***, $p<0.05$, $p<0.01$, <0.001 with ordinary one-way ANOVA with Tukey's multiple comparison test.

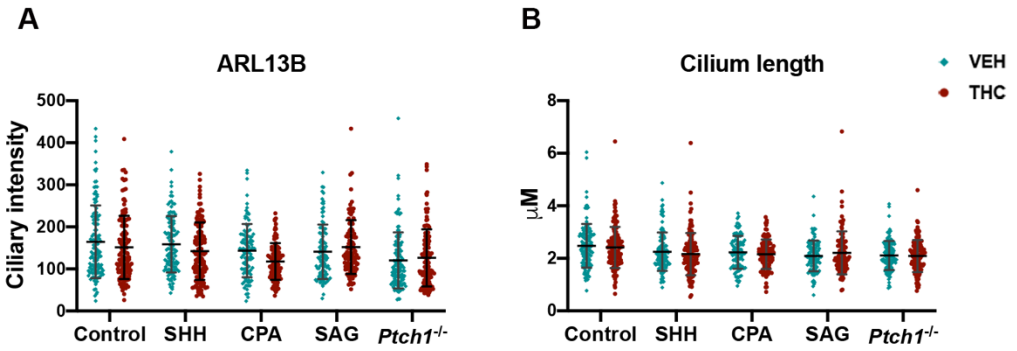

Fig. S4. THC does not grossly affect primary cilia.

A. Fluorescence intensity for the primary cilia marker, ARL13B.

B. Primary cilia length.

Each point represents an individual cell collated from at least 3 independent experiments.

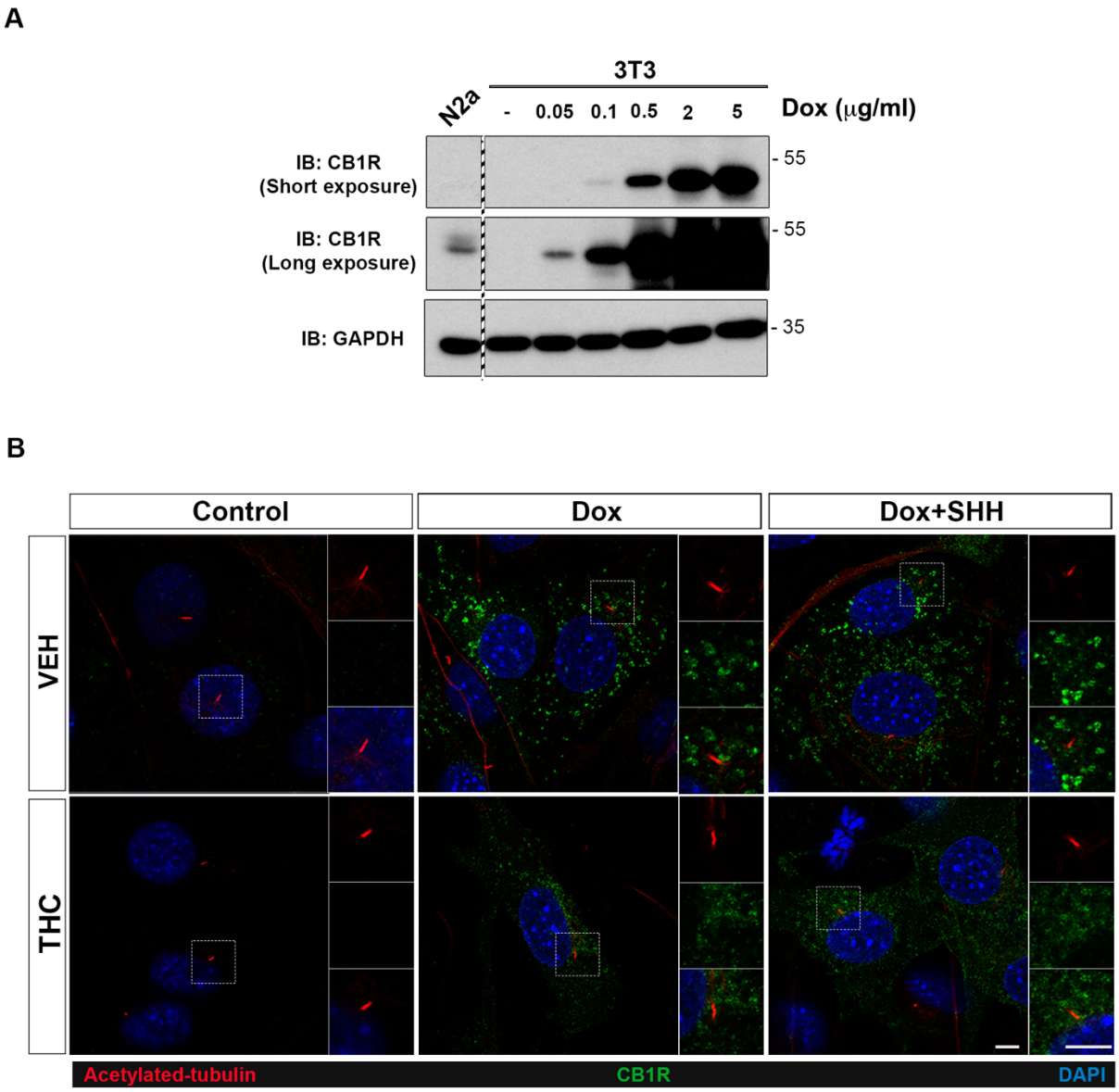

Fig. S5. NIH3T3 cells with inducible expression of CB1R.

A. NIH3T3 cells were infected with a lentiviral vector encoding doxycycline-inducible expression of CB1R. Cells were treated with the indicated doses of doxycycline (Dox) and harvested for western blot analysis 24 hours later. N2a, Neuro-2a cells, a cell line that expresses CB1R endogenously. The samples are from the same gel and membrane. The dashed region indicates lanes not shown. B. Exogenously expressed CB1R does not localize to primary cilia in NIH3T3 cells, with or without SHH stimulation. Primary cilia are marked by acetylated tubulin. Scale bars, 5 μm.

Table S1. Frequency of THC-induced HPE in *Cdon*$^{-/-}$ embryos. Related to Figure 1.

Treatment	# *Cdon*$^{+/+}$ or *Cdon*$^{+/-}$ embryos	# *Cdon*$^{+/+}$ or *Cdon*$^{+/-}$ embryos with HPE	# *Cdon*$^{+/-}$ embryos	# *Cdon*$^{-/-}$ embryos with HPE (%)	P value, Fisher's exact test (vs.VEH)
Vehicle	29	0	15	0	
THC (5 mg/kg)	33	0	12	2 (16.7)	>0.05
THC (10 mg/kg)	32	0	13	4 (30.8)	0.03
THC (15 mg/kg)	27	0	11	4 (36.4)	0.02

Table S2. Numbers of FOXA2^{+}, NKX2.2^{+}and OLIG2^{+} cells in the VNT. Related to Figure 2.

E9.5	*Cdon*$^{+/-}$ VEH	*Cdon*$^{+/-}$ THC	*Cdon*$^{-/-}$ VEH	*Cdon*$^{-/-}$ THC
FOXA2^{+} cells	24.5 ± 2.7	23.5 ± 2.8	24.1 ± 4.7	12 ± 2.1
NKX2.2^{+} cells	32.2 ± 4.5	32.8 ± 4.1	32.7 ± 7.1	20.4 ± 3.6
OLIG2^{+} cells	98.9 ± 15.4	106.3 ±26.5	97.8 ± 18.5	77.7 ± 20.7
Whole neural tube	317.8 ± 18.7	327.1 ±8.4	320.5 ± 14.1	307.4 ± 32.5

N=5 embryos for each group, 3-6 sections per mouse